The role of GABARAPL1 (GEC1) in autophagic flux and mitochondrial quality control in MDA-MB-436 breast cancer cells

Michaël Boyer-Guittaut,[1,2,3,*] Laura Poillet,[1] Qiuli Liang,[2,3] Elodie Bôle-Richard,[1,#] Xiaosen Ouyang,[2,3,4] Gloria A. Benavides,[2,3] Fatima-Zahra Chakrama,[1,&] Annick Fraichard,[1] Victor M. Darley-Usmar,[2,3] Gilles Despouy,[1] Michèle Jouvenot,[1] Régis Delage-Mourroux[1] and Jianhua Zhang[2,3,4,*]

[1]Université de Franche-Comté, Laboratoire de Biochimie, EA3922 Estrogènes, Expression Génique et Pathologies du Système Nerveux Central, SFR IBCT FED4234, Sciences et Techniques, 16 route de Gray, 25030 Besançon Cedex, France.
[2]Department of Pathology, [3]Center for Free Radical Biology, University of Alabama at Birmingham,
[4]Department of Veterans Affairs, Birmingham VA Medical Center, 901 19th Street South, Birmingham, AL 35294, USA.
[#]Current address: EFS B/F-C, INSERM, UMR 1098, Interactions Hôte-Greffon-Tumeurs & Ingénierie Cellulaire et Génique, 1 Bd A. Fleming, 25052 Besançon, France.
[&]Current address: Université de Lyon, Inserm U1052, CNRS UMR5286, Centre de Recherche en Cancérologie de Lyon, Centre Léon Bérard, 28 Rue Laennec, 69008 Lyon, France.

***Corresponding authors:** Jianhua Zhang, Ph.D., Department of Pathology, University of Alabama at Birmingham, BMRII-534, 901 19th Street S, Birmingham, AL 35294, USA, Phone: 205-996-5153; Fax: 205-934-7447; Email: zhanja@uab.edu
Michaël Boyer-Guittaut, Ph.D., Université de Franche-Comté, Laboratoire de Biochimie, EA3922, SFR IBCT FED4234, UFR-ST, 16 route de Gray, 25030 Besançon Cedex, France. Phone: 0033-3-81-66-69-58; Fax: 0033-3-81-66-69-70; Email: michael.boyer-guittaut@univ-fcomte.fr

Key words: GABARAPL1, GEC1, GABARAP, LC3, LAMP1, MDA-MB-436, mitochondria, lysosome, mitophagy, autophagy, breast cancer

Running Title: GABARAPL1 (GEC1) in autophagic flux and mitochondrial quality control

Abbreviations

ATG, autophagy-related protein; CQ, chloroquine; BafA1, bafilomycin A1; DNML1/Drp1, Dynamin-related protein 1; ECAR, extracellular acidification rate; FCCP, carbonyl cyanide 4-(trifluoromethoxy)phenylhydrazone; GABA, gamma-aminobutyric acid; $GABA_AR$, gamma-aminobutyric acid type A receptor; GABARAP, $GABA_A$-receptor associated protein; GABARAPL1, GABARAP-like 1; GABARAPL2, GABARAP-like 2; GATE-16, golgi-associated ATPase enhancer of 16 kDa; GEC1, glandular epithelial cell protein 1; GFP, green fluorescent protein; GSH, glutathione; HNE, 4-hydroxynonenal; KD, knock-down; MAP1-LC3, microtubule-associated protein 1 light chain 3; MFN1, mitofusin 1; MTT, 3-(4,5-dimethylthiazol-2-yl)-2,5-diphenyl tetrazolium bromide; NEM, N-ethylmaleimide; NBR1, neighbor of BRCA1; OCR, oxygen consumption rate; PBS, phosphate buffer saline; PBS-T, PBS-triton-X; PFA, paraformaldehyde; PPARGC1A, peroxisome proliferator-activated receptor gamma coactivator 1-alpha; PINK1, PTEN-induced putative kinase 1; PVDF, polyvinylidene difluoride; RCR, respiratory control ratio; SDS, sodium dodecylsulfate; SQSTM1/p62, Sequestosome 1/p62; TBS-T, tris buffer saline-tween; TMRM, tetramethylrhodamine methyl ester perchlorate; VDAC1, voltage-dependent anion-selective channel protein 1; WT, wild type.

Abstract

GABARAPL1/GEC1 is an early estrogen induced gene which encodes a protein highly conserved from *C. elegans* to humans. Overexpressed GABARAPL1 interacts with $GABA_A$ or kappa opioid receptors, associates with autophagic vesicles, and inhibits breast cancer cell proliferation. However, the function of endogenous GABARAPL1/GEC1 has not been extensively studied. We hypothesized that GABARAPL1 is required for maintaining normal autophagic flux, and plays an important role in regulating cellular bioenergetics and metabolism. To test this hypothesis, we knocked down *GABARAPL1* expression in the breast cancer MDA-MB-436 cell line by shRNA. Decreased expression of GABARAPL1 activated pro-cancer responses of the MDA-MB-436 cells including increased proliferation, colony formation and invasion. In addition, cells with decreased expression of GABARAPL1 exhibited attenuated autophagic flux and decreased number of lysosomes. Moreover, decreased GABARAPL1 expression led to cellular bioenergetic changes including increased basal oxygen consumption rate, increased intracellular ATP, increased total glutathione, and an accumulation of damaged mitochondria. Taken together, our results demonstrate that GABARAPL1 plays an important role in cell proliferation, invasion, autophagic flux, as well as mitochondrial homeostasis and cellular metabolic programs.

Introduction

The *GEC1* (*Glandular Epithelial Cells 1*) gene was discovered during the search for new early estrogen-induced genes in a model of guinea-pig glandular epithelial cells.[1] The encoded protein is conserved throughout evolution from *C. elegans* to humans, with 100% identical protein sequence from yeast to mammals.[2] This protein also shares a high degree of homology with the GABARAP protein, which expresses a new $GABA_A$ receptor-associated protein.[3] The two proteins share 87% sequence identity, a common tridimensional structure similar to the one described for ubiquitin,[4] and serves a similar function in $GABA_A$ receptor transport.[5] In addition, GEC1 was shown to interact with tubulin and promote tubulin assembly and microtubule bundling *in vitro*.[5] GEC1 was later renamed GABARAPL1 for $GABA_A$ receptor-associated protein-like 1. The role of GABARAPL1 in the transport of receptors is not restricted to the $GABA_A$ receptor since it has been shown to interact with the human kappa opioid receptor and enhance its trafficking to the plasma membrane.[6]

In rodents, *GABARAPL1* is highly expressed in the brain, and restricted to neurons.[7-9] In muscle or cardiomyocytes, it is activated after glucose deprivation, oxidative stress or ultra-endurance exercise.[10, 11] In most tumor cell lines or cancer tissues tested, *GABARAPL1* expression is lower than non-cancerous tissues or cells.[12, 13] Inhibition of *GABARAPL1* expression has also been observed in muscles of Duchenne muscular dystrophy patients,[14, 15] in the skeletal muscle of patients presenting an upper motor neuron lesion[15] or in the *substantia nigra* of Parkinson disease patients.[16] Whether the changes of *GABARAPL1* expression are contributing to the disease pathogenesis or compensatory responses to various pathological conditions is currently unclear.

Recently, we demonstrated that GABARAPL1, like GABARAP, can associate with autophagic vesicles and is involved in the autophagy process.[2] The autophagy pathway is a

cellular degradation pathway involved in the degradation of long-lived proteins and organelles.[17-21] This is in contrast to the proteasome pathway which is involved in the specific degradation of ubiquitinylated short-lived proteins.[22] Autophagy requires more than thirty ATG proteins (AuTophaGy-related genes) and the regulated formation of a double membrane structure known as the phagophore. Following its initiation, this structure elongates and engulfs part of the cytoplasm containing organelles, aggregates or soluble proteins, to form a closed vesicle called the autophagosome. This vesicle will later fuse with the lysosomes, to form an autophagolysosome, and induce the degradation of its content and is involved in maintaining mitochondrial quality and in the responses to oxidative stress.[23-25] The initiation and the elongation of this structure requires several ATG proteins, and homologues of the yeast ATG8, which are conjugated to phospholipids of the elongating double membrane structure *via* a cycle similar to the one described for the ubiquitinylation of proteins.[22] These ATG8 homologues are divided into two subfamilies: the MAP-LC3 (microtubule-associated protein light chain 3) and the GABARAP family which comprises LC3A, B and C and GABARAP, GABARAPL1, GABARAPL2, respectively. These proteins were initially believed to serve redundant functions in the formation of the autophagosome.

Recent studies have shown that in HeLa cells, the proteins of the LC3 family are indispensable for the elongation of the double membrane structure while the GABARAP family members are required for the late maturation of the autophagosomes.[26] In the course of these experiments, siRNA directed against each of the 6 *ATG8* homologues inhibited SQSTM1/p62 degradation. However, cross regulation among individual siRNAs was not examined. Out of the 6 *ATG8* family genes, *Lc3b* and *Gabarap* genes have been knocked out in mice. Mice with disruption of the *Gabarap* or the *Lc3b* gene alone have been shown to be viable and without an apparent change in phenotype.[27, 28] It is noteworthy that, alterations of the autophagy pathway have not been reported with the *Gabarap* knockout mice. The facts that these animals are viable,

fertile and do not exhibit any noticeable phenotype are in favor of the redundancy theory. Recent studies, however, have shown that *Lc3b* KO mice exhibited decreased autophagic vesicles in the lung after chronic exposure to cigarette smoke, suggesting that in response to specific stimulus, individual *ATG8* homologs may play important and distinct roles in autophagy.[29]

Consistent with these observations, one recent hypothesis to explain the high number of ATG8 homologues in mammals is their possible involvement in different types of selective autophagy (e.g. aggrephagy, mitophagy, pexophagy, ribophagy or xenophagy).[30] Adapter proteins, such as SQSTM1, NBR1 (Neighbor of BRCA1), and NIX/BNIP3L, interact with ubiquitinylated aggregates or organelles *via* their ubiquitin associated (UBA) domains and recruit cargos to the autophagosomes by interacting with different ATG8 members *via* their LIR domain (LC3-interacting domain, W/YxxL/I). Several studies have indicated that the distinct ATG8 family members have different affinities for the specific cargos and therefore might be the missing link to explain the selectivity of the autophagy process. For example, it has been shown that all ATG8 members can bind NIX *in vitro* but only GABARAPL1 is preferentially recruited to damaged mitochondria in a NIX-dependent manner in cells treated with the mitochondrial uncoupler CCCP.[31] Another study showed that GABARAPL1 can specifically bind to STBD1 (Starch binding domain-containing protein 1)/genethonin1 and induce glycogen degradation by autophagy in a process now known as glycophagy.[32] This process is also dependent on the Stbd1 LIR domain and seems to be specific to GABARAPL1.[33] A third study recently demonstrated that GABARAPL1 inhibits Wnt/β-catenin signaling in MCF-7 cells *via* the selective degradation of the protein Dishevelled 2 (DVL2), an activator of the Wnt/β-catenin pathway.[34] In addition, overexpression of GABARAPL1 inhibits MCF-7 cell proliferation and the formation of tumors in nude mice.[34] Whether the role of GABARAPL1 in regulating cell proliferation and tumor formation is linked to the degradation of DVL2 or the autophagy pathway has not been determined. These observations suggest that different ATG8 members may be involved in

selective autophagy processes linked to the degradation of specific cargos, occurring in distinct cell types or tissues or in response to different stressors.

Since GABARAPL1 has been shown to be involved in glycogen degradation, relocalized to damaged mitochondria and interacting with NIX, we hypothesized that GABARAPL1 may play an essential role in cell metabolism and in particular in energy production. This function may also explain the fact that overexpression of this protein inhibits MCF-7 breast cancer cell proliferation and tumor formation.[13, 34] Indeed, it is known that highly proliferating breast cancer cells need increased levels of ATP and that tumor formation requires an active autophagy pathway to survive under hypoxic and oxidative stress before the vascularization of a solid tumor.[35]

In this study, we stably expressed five different shRNAs targeting *GABARAPL1* in the MDA-MB-436 cell line which is the only breast cancer cell line, to our knowledge, that has detectable levels of the protein. This protocol allowed us to select cell lines targeting only GABARAPL1, without affecting GABARAP or LC3B, and study the function of this knock-down on the phenotype of breast cancer cells. Our data showed that several shRNAs specific to *GABARAPL1* decreased mRNA expression but only two significantly decreased levels of the GABARAPL1 protein. These stable cell lines exhibited increased cell growth, decreased autophagic flux, and decreased lysosome number. Furthermore, decreased GABARAPL1 led to increased glutathione (GSH) and ATP, increased basal respiration as well as increased numbers of mitochondria. These observations support the hypothesis that the lower levels of GABARAPL1 in cancer cells inhibits autophagic flux and thereby the turnover of mitochondria leading to their accumulation and an increase of basal respiration, levels of ATP and GSH. This increased energetic and antioxidant capacity in response to the suppression of GABARAPL1 could then contribute to more aggressive phenotypes in cancer cells.

Results

Establishment of GABARAPL1 knock-down stable cell lines

MDA-MB-436 cells were transfected with five different shRNA-*GABARAPL1*-expressing vectors (directed against the open reading frame of the gene) and a shRNA-*control*-expressing vector, and we selected five antibiotic-resistant clones for each shRNA. Cells with stable transfection of shRNA-*GABARAPL1* sh2 exhibited the greatest decrease in the mRNA (80%) (**Fig. 1A**) and protein expression (96%) levels (**Fig. 1B-C**) compared to the control cell line expressing the shRNA control (shC), without changing *GABARAP* and *LC3B* mRNA levels. In a second cell line, cells with stable transfection of shRNA-*GABARAPL1* sh5 exhibited a 50% decrease of GABARAPL1 mRNA (**Fig. 1A**) and an 80% decrease in protein levels (**Fig. 1B-C**).

GABARAPL1 regulates MDA-MB-436 proliferation, colony formation ability and cell invasion

We investigated whether the decrease of GABARAPL1 expression in the MDA-MB-436 cell line would alter its tumor cell-linked features such as proliferation, colony formation and invasion. We first performed an MTT assay over an 8-day period to determine whether GABARAPL1 regulated cell proliferation. We observed that the sh2 and sh5 cell lines exhibited an increased proliferation rate compared to the shC control cell line (**Fig. 2A**). We also confirmed that this increase was not due to a decrease in cell death (data not shown). That the sh5 cell line exhibiting a lower increase in proliferation compared to the sh2 cells is consistent with the observation that *GABARAPL1* is decreased by 80% in sh5 compared to 96% in sh2 cells (**Fig. 1C**). We then assessed the ability of the sh2 cell line to form new colonies. As shown in **Fig. 2B**, after 14 days, we found a significantly higher number of colonies formed with the sh2 cell line compared to the shC cell line. Furthermore, using a modified Boyden chamber, we found that the sh2 cells exhibited a substantially higher capacity for migration (**Fig. 2C**). We have also tested

the ability of the sh5 cells to form new colonies and migrate in a Boyden chamber but did not detect any significant change compared to the control cells (Data not shown). This can be explained by the fact that the decrease of *GABARAPL1* in the sh5 cells is less than that observed in the sh2 cells.

GABARAPL1 knock-down inhibits autophagic flux

We have previously shown that GABARAPL1 associates with autophagosomes.[2] To investigate whether loss of GABARAPL1 alters autophagic flux, we quantified the levels of LC3-II, the autophagosome-associated form of the protein, in the absence and presence of the lysosomal inhibitor chloroquine, in the three cell lines, shC, sh2 and sh5. We found that the basal levels of LC3-II were not significantly changed by suppressing the levels of GABARAPL1 in sh2 but were increased in sh5 cells (**Fig. 3A**, comparing lanes 1-3 and 7-9, $p<0.05$ comparing LC3-II/ACTIN between shC and sh5 cells). We calculated the ratio between the LC3-II levels with and without chloroquine as an index of overall autophagic flux,[36] and observed a decrease of this ratio in the sh2 and sh5 cell lines compared to the control cells (**Fig. 3B**). These data indicate that a loss of GABARAPL1 results in a decrease in autophagic flux. To determine whether this attenuation of autophagic flux was due to an inhibition of autophagy induction or the degradation of autophagosomes, we first examined MTOR activation. We found that MTOR and p70S6K phosphorylation levels were similar in the shC and sh2 cell lines (**Fig. 3C** and **D**). Moreover, both shC and sh2 cells increase autophagic flux in response to rapamycin, a MTOR-dependent inducer, as indicated by an increase of LC3-II levels (**Fig. S1A-C**). Autophagic flux as defined by the ratio LC3-II in response to rapamycin+CQ/LC3-II in response to rapamycin is similar in shC and sh2 cells (**Fig. S1D**). However the flux in the presence of rapamycin and in the absence of rapamycin is similar in shC cells, and significantly increased in sh2 cells (**Fig. 3B**, which is also included in **Fig. S1D** for direct comparison). In contrast, sh2 cells exhibited a greater increase in

LC3-II in response to trehalose, a MTOR-independent autophagy inducer, compared to shC cells, and no further increase in LC3-II when both trehalose and chloroquine were present (**Fig. S2A-C**). Hence, the sh2 cell line exhibited a lower increase of autophagic flux in response to trehalose compared to shC cells (**Fig. S2D**). These data suggest that GABARAPL1 knock-down does not change MTOR signaling, but changes the autophagic response to rapamycin.

Both rapamycin and trehalose inhibited sh2 cell proliferation (**Fig. S3A, B**). As shown in **Fig. S1** and **S2**, autophagic flux was increased in sh2 cells in response to rapamycin, whereas it was unchanged in response to trehalose. Therefore, the inhibition of proliferation by rapamycin or trehalose cannot be simply attributed to an increase in autophagic flux. Consistent with this interpretation, we found no change in cell proliferation for sh2 cells following transfection of *ATG7* or non-targeting siRNA (**Fig. S3C** and **D**), despite a significant knockdown of *ATG7*, suggesting that further inhibition of autophagy in sh2 cells does not affect proliferation.

GABARAPL1 knock-down increases *SQSTM1* mRNA, SQSTM1 protein, as well as BECN1 protein levels

Since we did not detect any change in MTOR signaling associated with GABARAPL1 knock-down, we examined the levels of other key proteins in the autophagic-lysosome pathway and found an increase of BECN1/Beclin1 and SQSTM1 protein levels in the sh2 and sh5 cells (**Fig. 4A** and **B**). Since the transcription of genes encoding these proteins may change according to the stress status of the cells,[37] we performed quantitative real-time RT-PCR, and found a significant increase in *SQSTM1* (about 4 fold) but not *BECN1* mRNA levels (**Fig. 4C**). Therefore, increased transcription of SQSTM1 in response to the loss of *GABARAPL1* may have contributed to the changes in its protein levels. Nevertheless, the loss of *GABARAPL1* also attenuated autophagic flux. To determine whether SQSTM1 protein also accumulates in sh2 cells independent of transcription, we transfected shC and sh2 cells with a pCMV-HA- SQSTM1

construct, in which *SQSTM1* expression is under the control of a constitutive CMV promoter. Our data showed a 50% increase in HA- SQSTM1 levels in the sh2 cells compared to the shC cells (**Fig. 4D** and **E**). These results suggest that both an increase of transcription and a decrease of autophagic flux contribute to the higher levels of SQSTM1 in sh2 cells.

GABARAPL1 knock-down decreases *LAMP1* mRNA and protein levels

Next we examined lysosome protein levels in shC, sh2 and sh5 cells. We found a significant decrease of LAMP1 (by 50%) in sh2 cells but not sh5 cells (**Fig. 5A** and **B**). The decreased LAMP1 protein in sh2 cells may be due to decreased transcription as *LAMP1* mRNA levels were also decreased by 30% in sh2 cells (**Fig. 5C**). Interestingly, both sh2 and sh5 cells exhibited significant decrease of LAMP1 immunostaining compared to shC cells (**Fig. 5D**). This discrepancy between LAMP1 western blot analyses and LAMP1 immunostaining may be due to a difference in protein denaturation procedure in western blotting and in immunostaining. Intriguingly, a decrease of LAMP1 protein level is not associated with a decrease of lysosomal protease activities. We found that lysosomal Cathepsin B activity and protein levels are unchanged, whereas Cathepsin D activity and protein levels are increased, in sh2 cells compared to shC cells (**Fig. S4A-C**). This increase of Cathepsin D may be a compensatory response to a decrease of LAMP1, as prior studies reported that a decrease in lysosome number led to the induction of Cathepsin activities.[38, 39]

GABARAPL1 knock-down increases mitochondrial membrane potential and the demand for mitochondrial bioenergetics

To determine the effects of GABARAPL1 on mitochondrial membrane potential we used TMRM staining and found a significant increase in the sh2 cells compared to shC cells, and decreased to the same levels by FCCP as expected (**Fig. 6A**). In addition, Mitotracker red

staining (**Fig. 6B**) was also increased in the sh2 cell line, consistent with either an increase in mitochondrial membrane potential or mitochondrial number. Similarly, Mitotracker intensity is higher in both sh2 and sh5 cells compared to shC cells as assessed by confocal microscopy (**Fig. 6C-D**).

We then used Seahorse XF24 analyzer to determine whether GABARAPL1 knock-down changed mitochondrial function.[24, 40] The shC and sh2 cells were plated at similar confluency (**Fig. 7A**). We then monitored the basal levels of oxygen consumption rate (OCR), and OCR following injection of oligomycin, an inhibitor of ATP synthase, FCCP, an uncoupler, and antimycin A, an inhibitor of mitochondrial complex III (**Fig. 7B**). We were then able to calculate Basal, ATP-linked, proton leak (non-ATP linked), Maximal, Reserve capacity and Non-mitochondrial OCR (**Fig. 7C**).[24, 40, 41] We found an increase in basal OCR in sh2 cells, which was largely due to an increase in non-ATP linked proton leak respiration, consistent with a higher membrane potential. We also determined the extracellular acidification rate (ECAR), which can be ascribed to glycolysis and other proton generating processes in the cells, but detected no differences between the two cell lines (**Fig. 7D**). Furthermore, we did not observe any changes of maximal OCR or reserve capacity (**Fig. 7C**), nor the State apparent (**Fig. 7E**), in response to GABARAPL1 knock-down, however, the RCR basal and maximal were decreased in sh2 cells compared to shC cells (**Fig. 7E**). Interestingly, we found that GABARAPL1 suppressed cells had higher amounts of ATP compared to the control cells suggests that the mitochondrial population in these cells is capable of meeting the increased demands for proliferation through increased metabolic activity (**Fig. 7F**).

GABARAPL1 knock-down leads to an increase of mitochondrial protein levels and an increase of damaged mitochondrial DNA

An altered autophagy-lysosome pathway may result in an increased mitochondrial number

in GABARAPL1 knock-down cells. We then examined whether the levels of proteins involved in mitochondrial biogenesis or homeostasis would be altered in sh2 cells. We found that levels of both PGC1α which is involved in mitochondria biogenesis,[42] and VDAC1, which is involved in the flux of metabolites to and from the mitochondria,[43] were up-regulated in sh2 cells compared to shC cells (**Fig. 8A** and **B**). Levels of MFN1 (Mitofusin 1), which is involved in mitochondria fusion,[44] DNML1/Drp1 (Dynamin-related protein 1), which is involved in mitochondria fission,[45] PINK1 and PARKIN, which are involved in mitophagy,[46] were unchanged. Our data support the hypothesis that GABARAPL1 is important in maintaining mitochondrial homeostasis by promoting autophagic flux, independent of mitochondrial fission/fusion or selective mitophagy.

As an additional index of mitochondrial number we measured mtDNA copy number relative to the genomic DNA. As shown in **Fig. 8C**, we found increased levels of mtDNA in sh2 cells compared to shC cells. These data also suggest that the both an attenuation of autophagic flux and an increase in mitochondrial biogenesis via PGC1α increase[42] may contribute to an increased MitoTracker staining, mtDNA copy number, mitochondrial membrane potential, and VDAC1 protein levels. To further assess mitochondrial health, we measured mtDNA damage, and found that sh2 cells exhibited significantly higher mtDNA damage compared to shC cells (**Fig. 8D**). mtDNA copy number is increased in sh5 cells compared to shC but mtDNA damage in sh5 is comparable to shC, this may reflect an incomplete GABARAPL1 knockdown in sh5 cells (data not shown).

The accumulation of mitochondria and the changes of mitochondrial quality suggest a defect in mitochondrial clearance in sh2 cells. To quantify mitochondrial clearance, we have performed co-staining of mitochondria and lysosomes in the presence or absence of FCCP (**Fig. S5**). We found a slight increase of MitoTracker/LysoTracker co-localization in sh2 cells compared to shC cells, this may be due to an increase of mitochondrial number, and is not consistent with

an attenuated selective mitophagy. We did not find a significant difference of FCCP-induced co-localization of mitochondria and lysosomes in shC or sh2 cells. Similarly, we did not find co-localization of GFP-PARKIN with mitochondria in shC or sh2 cells (data not shown) but it is conceivable that the potential defects in mitochondrial clearance in sh2 cells are independent of Parkin translocation to the mitochondria. The exact mechanism of how accumulation of underperforming mitochondria occurs in sh2 cells remains unclear.

GABARAPL1 knock-down promoted cell survival in response to HNE

We incubated shC and sh2 cells with increasing concentrations of HNE, a product of lipid peroxidation previously described to decrease mitochondrial activity,[40, 41, 47] through its modification of proteins including the ATP synthase β subunit[48] or sirt3.[49] As shown in **Fig. 9A**, after 16 h, the viability of sh2 cells was higher than shC cells after incubation with different concentrations of HNE, indicating that GABARAPL1 knock-down enhances cell survival in response to HNE.

To determine effects of HNE on autophagic flux in sh2 cells, we assessed the LC3-II levels (**Fig. 9B** and **C**). We found that LC3-II levels were significantly increased in the shC cells (~1.4 fold) but unchanged in sh2 cells following HNE exposure. Consequently, the ratio of LC3-II with HNE versus LC3-II without HNE was also lower in the sh2 cells. Basal HNE-protein adducts were higher in sh2 cells compared to shC cells (**Fig. 9D** and **E**) (compare lanes 1-3 and 4-6). After exposure to exogenous HNE, HNE-protein adduct levels increased to 1.5 fold in the shC cells but did not change in the sh2 cells (**Fig. 9D** and **E**). Next we determined the levels of GSH in the two cell lines, since the formation of HNE-protein adducts could be attenuated by intracellular cellular glutathione (GSH) which can detoxify HNE through the action of glutathione transferases.[50] As shown in **Fig. 9F**, GSH levels were significantly higher in the sh2 cell lines, suggesting that the decreased HNE-induced cell death in sh2 cells may be partially provided by

the higher levels of GSH.

Discussion

Recent studies have shown that GABARAPL1 is associated with autophagic vesicles[2] and the *GABARAPL1* gene may be a tumor suppressor gene and a prognostic biomarker in breast cancer.[13] GABARAP, the closest homologue of GABARAPL1, is expressed at low levels in invasive ductal and invasive lobular carcinomas compared with normal breast tissue, and the overexpression of GABARAP in CAL51 decreased their proliferation rate as well as their ability to form colonies in soft-agar and to form tumors in nude mice.[51] GABARAPL1 overexpression has been shown to inhibit proliferation of the breast cancer cell line (MCF-7),[13] and their ability to form tumors in nude mice.[34] Building on these data, we hypothesized that endogenous GABARAPL1 plays a role in suppressing the cancer cell phenotype and in mediating autophagy. In this study, we established stable cell lines that exhibited significant loss of *GABARAPL1* mRNA and protein levels (**Fig. 1**), and found that these cells exhibited an increased proliferation rate, colony formation and invasion (**Fig. 2**) consistent with the hypothesis that *GABARAPL1* is a tumor suppressor gene.

Autophagy plays a complex role in tumor initiation and progression. On the one hand, autophagy protects against the production of reactive oxygen species in the cells and their deleterious effects in mutating DNA and promoting cell transformation.[35] On the other hand, autophagy is required for the transformation of mouse embryonic fibroblasts by the Ras oncogene and this effect is linked to its role in nutrient recycling such as glucose uptake and increased glycolytic flux.[52] During the later stages of *in vivo* tumor formation, autophagy has been shown to be necessary for the cancer cell survival in hypoxia before the vascularization of the tumor.[35] Autophagy has also been shown to protect against cellular stress induced by the chemotherapeutic drugs used in cancer treatment leading to several clinical trials involving the

use of an inhibitor of the autophagy flux as a combination therapy.[53] Even though the mechanism is still unclear, many studies suggest a role of autophagy in the regulation of cancer cell metabolism allowing them to meet the requirements for rapid proliferation. Using multiple autophagic flux analyses, including comparing LC3-II levels with and without chloroquine, endogenous *SQSTM1* mRNA and protein levels, as well as exogenous constitutively expressed pCMV-HA-SQSTM1 (**Fig. 3A** and **B, Fig. 4D** and **E**), we have found that GABARAPL1 knock-down cells exhibit a decreased autophagic flux. Interestingly, sh5 cells with incomplete in GABARAPL1 knock-down also exhibited decreased autophagic flux, although to a less extent than sh2 cells and did not result in the same colony formation and migration phenotypes as the sh2 cells.

The underlying mechanism of attenuated autophagic flux as a result of GABARAPL1 knock-down appears to be a significant decrease of LAMP1 protein levels and lysosome number (**Fig. 5A-D**), supporting the hypothesis of that loss of GABARAPL1 leads to an attenuation of autophagosomal degradation. Importantly, we found no difference in the phosphorylation of MTOR and p70S6K between control and GABARAPL1 knock-down cells, suggesting an MTOR independent attenuation of autophagic flux (**Fig. 3C** and **D**). Furthermore, we found increased BECN1 levels that cannot explain an attenuation of autophagic flux (**Fig. 4A-C**). Previous studies have shown that autophagy and lysosomal genes are coordinately regulated by master transcription activators and repressors, [54-56] such coordinate regulation appears to be perturbed in GABARAPL1 knock-down cells. In this context, it has been previously shown that rapamycin and trehalose are able to induce TFEB (Transcription Factor E-B), a transcription factor specifically inducing the transcription of genes involved in the autophagosomal and lysosomal biogenesis including LAMP1.[54, 55] We found that rapamycin and trehalose inhibited cell proliferation and abolished the effects of GABARAPL1 suppression on cell proliferation. The effects of rapamycin and trehalose on cell proliferation may be linked to an increase in LAMP1.

Furthermore, although the exact mechanisms are unclear, our observation that LAMP1 is decreased and Cathepsin D is increased in sh2 cells are consistent with prior findings and support a differential role of lysosomal components in cell proliferation.[57, 58, 59]

GABARAP1 has been previously linked to the selective autophagy of mitochondria, shown to interact with NIX, a mitochondrial protein, and recruited to mitochondria to induce their clearance during the maturation of reticulocytes.[31] Because mitophagy has been shown to degrade damaged mitochondria and therefore suppresses reactive oxygen species formation and DNA damage, and that our results showed that autophagic flux is attenuated in the absence of GABARAPL1, we determined whether GABARAPL1 knock-down would lead to desensitization to mitochondrial stressor-induced autophagy. Indeed, we found that in response to HNE, which is a by-product of lipid peroxidation previously shown to modify mitochondrial proteins and inhibit their activity,[24, 41, 48] GABARAPL1 knock-down cells exhibit less of increase in LC3-II levels compared to control shC cells (**Fig. 9B** and **C**). However, cell survival in response to HNE is dependent of GABARAPL1 (**Fig. 9A**). Further, GABARAPL1 knock-down induced a higher level of total endogenous HNE-protein adducts in the cells, and there were no further increase after additional HNE exposure in these cells (**Fig. 9D**). Additionally, glutathione steady state levels are increased in the GABARAPL1 knock-down cells compared to control cells (**Fig. 9G**), and the higher level of glutathione may form conjugates with the exogenously added HNE to inhibit its toxic effect in the cells.[60] The increase of endogenous HNE-protein adducts may be due to the attenuation of autophagic flux, and the increased adducts may also signal to induce anti-oxidant response for the cells to produce more enzymes involved in glutathione synthesis.[61]

We also determined the impact of GABARAPL1 knock-down on mitochondrial function. We found that GABARAPL1 knock-down cells exhibited increased mitochondrial membrane potential, mitochondrial biogenesis factor PPARGC1A, mitochondrial protein VDAC1, both total and damaged mtDNA (**Fig. 6**-**8**). In addition to exhibiting decreased autophagic flux as discussed

above (**Fig. 4**), sh5 cells with incomplete in GABARAPL1 knock-down also exhibited increased total mtDNA but not damaged mtDNA (**Fig. 8**), suggesting that autophagic flux and accumulation of mitochondrial mass are sensitive to moderate change of GABARAPL1 levels, whereas increased colony formation, cell migration/invasion, and mtDNA damage occur only when GABARAPL1 level decreases more than 70% (**Fig. 1**).

These competing impacts on mitochondrial homeostasis due to *GABARAPL1* knock-down resulted in a cellular bioenergetic profile that did not substantially deviate from that of the control shC cells, other than a significant increase in proton leak (**Fig. 7**). Importantly, ATP levels were increased in response to GABARAPL1 inhibition showing that although a decrease in mitochondrial quality occurred, the overall mitochondrial population was still competent to meet the energetic demands of the cell. This could be due to the activation of mitochondrial biogenesis in attempt to restore the integrity of the mitochondrial population and a small but active population of functioning mitochondria.

Our study support the model that GABARAPL1 inhibition induces a depletion of LAMP1 and lysosomal number, attenuates autophagic flux, and leads to an accumulation of damaged mitochondria, associated with stimulated mitochondrial biogenesis leading to increased mitochondrial number, mitochondrial protein, mitochondrial membrane potential, mitochondrial respiration, and ATP levels (**Fig. 10**). The increase of mitochondrial number and cellular glutathione, which itself could be stimulated by an increase in the basal levels of mitochondrial reactive oxygen species, further resulted in resistance to cell death, and may contribute to increased proliferation and aggressiveness of these cells. Our data demonstrate that GABARAPL1 plays an important role in regulating the autophagy-lysosome pathway, mitochondrial activity, cell metabolism and proliferation.

Materials and Methods

Reagents and antibodies

Cell culture reagents were purchased from Invitrogen (Carlsbad, CA). The following antibodies were used: polyclonal anti-GABARAPL1 (Proteintech, 11010-1-AP, 1:1,000), polyclonal anti-LC3B (Sigma-Aldrich, L8918, 1:3,000), monoclonal anti-SQSTM1/p62 (Abnova, H00008878-M01, 1:3,000), monoclonal anti-LAMP1 (Developmental hybrid studies, H4a3, 1:1000), monoclonal anti-VDAC1 (Abcam, ab16816, 1:1000), monoclonal anti-DNML1/Drp1 (Abcam, ab56788, 1:1000), polyclonal anti-MFN1 (Santa Cruz, H65 sc-50330, 1:1000), polyclonal anti-PPARGC1A (Santa Cruz, H300 sc-13067, 1:1000), monoclonal anti-PINK1 (Abcam, ab23707, 1:1000), polyclonal anti-PARKIN (Santa Cruz, H300 sc-30130, 1:1000), goat anti-4-HNE (Alpha diagnostics, HNE12-S, 1:3000), polyclonal rabbit anti-MTOR (Cell signaling, 2983, 1:1000), polyclonal rabbit anti-phospho-MTOR (Cell signaling, 2971, 1:1000), polyclonal rabbit anti-p70S6K (Cell signaling, 9202, 1:1000), polyclonal rabbit anti-phospho-p70S6K (Cell signaling, 9205, 1:1000), polyclonal rabbit anti-Cathepsin B (Santa Cruz, sc-13985, 1:1000), polyclonal goat anti-Cathepsin D (Santa Cruz, sc-6486, 1:1000), and monoclonal anti-ACTIN (Sigma-Aldrich, 1:10,000). Bafilomycin A1 (Sigma, B1793) was prepared as a 50 μM stock in DMSO. Rapamycin (Sigma-Aldrich, R8781) was purchased as a 2.74 mM stock in DMSO. Chloroquine (Sigma-Aldrich, C6628) was prepared as a 200 mM stock in water. Tetramethylrhodamine methyl ester perchlorate (TMRM, Sigma-Aldrich, T5428) was prepared as a 100 mM stock in DMSO. 3-Methyladenine (3-MA, Sigma-Aldrich, M9281) was prepared fresh as a 10 mM working solution in complete culture medium. Oligomycin (O4876), FCCP (C2920) and antimycin A (A8674) were purchased from Sigma-Aldrich. 4-hydroxynonenal (HNE) was prepared fresh from a stock solution purchased from Calbiochem (393204). The HA-SQSTM1 expressing vector has been purchased from Addgene (28027, Dr. Qing Zhong).

Cell culture and stable cell lines

The MDA-MB-436 cell line (ATCC) was maintained in DMEM medium (Dulbecco's Modified Eagle's Medium, Invitrogen, 11965-092) containing 1 mM L-Glutamine and supplemented with 10% fetal bovine serum (FBS, Atlanta Biologicals, S111-50), 100 µg/ml Penicillin/Streptomycin (Invitrogen, 15140-122) and 1 mM Sodium Pyruvate (Invitrogen, 11360-070) in a 5% CO_2 incubator at 37°C. Cells were split every four days (1:3 dilution). The MDA-MB-436-shRNA-*control* (shC or control) and –*GABARAPL1* (sh2 or GABARAPL1 KD) cell lines were maintained in complete medium supplemented with 1 µg/ml puromycin (Invitrogen, 28-111-QL). To create these stable cell lines, MDA-MB-436 cells (10^6) plated in 10 cm-diameter cultures dishes were transfected the day after plating using 10 µg of five different pKo.1-puro-shRNA-*GABARAPL1* vectors (Mission shRNA, Sigma-Aldrich, SHCLNG-NM_031412, shRNA 443s1c1) and one pKo.1-puro-shRNA-*control* vector (Sigma-Aldrich, SHC002) and 20 µl TransFast reagent (Promega, E2431) according to the manufacturer's protocol. After 48 h incubation, 3 µg/ml puromycin was added to each plate and the medium was changed every two days for the next 14 days until the appearance of antibiotic-resistant single clones. Five resistant clones for each shRNA transfection were then tested for the expression of *GABARAPL1*, *GABARAP* and *LC3B* mRNAs and proteins by qRT-PCR and western-blotting, respectively. The stable cell lines used later on in this study are the MDA-MB-436-shRNA-*control* clone 2 (shC or control) and the MDA-MB-436-shRNA-*GABARAPL1* clone 2 (sh2 or GABARAPL1 KD). The sh5 clone has been designed using the same protocol as described for the sh2 clone but using a different shRNA (Mission shRNA, Sigma-Aldrich, SHCLNG-NM_031412, shRNA 570s1c1).

Quantitative real-time RT-PCR analysis

Total RNAs were extracted using the TRI Reagent (Invitrogen, AM9738). To remove any

genomic DNA contamination, total RNAs were treated with RNAse-free DNAse I (Invitrogen, AM2222) and purified with phenol/chloroform. A volume of 1 µg of total RNAs was reverse transcribed using M-MLV RT (Sigma-Aldrich, M1302) and oligo(dT)15 primers following the manufacturer's instructions. Quantitative PCR was run on the Step One Real Time PCR System (Applied Biosystems) using the SYBER Green PCR Master Mix (Applied Biosystems, 4309155) and the following parameters: 10 min at 95°C followed by 40 cycles: 15 sec at 95°C and 1 min at 60°C. The target genes levels (*GABARAPL1*, *GABARAP*, *LC3B, LAMP1, SQSTM1, and BECN1*) were normalized to the levels of the *H3B2* housekeeping gene (forward: 5'-GCTAGCTGGATGTCTTTTTGG-3' and reverse: 5'-GTGGTAAAGCACCCAGGAAA-3'). The primer sequences were: *GABARAPL1* (5' CCCTCCCTTGGTTATGATCCA-3' and 5'-AGGAAGGGATTGCTGGGTTCT-3'), *GABARAP* (5'-ACTCCCACCCCACAAAATCC-3' and 5'-GCCTTTCCCATCCTGCTGTA-3'), *LC3B* (5'-CGGAAAGCAGCAGTGTACCA-3' and 5'-GGCAGAAGGGAGTGTGTCTGA-3'), *LAMP1* (5'-GTGTCTGCTGGACGAGAACA-3' and 5'-ATGAGGACGATGAGGACCAG-3'), *SQSTM1* (5'-AAATGGGTCCACCAGGAAACTGGA-3' and 5'-TCAACTTCAATGCCCAGAGGGCTA-3') and *BECN1* (5'-TCACCATCCAGGAACTCACA-3' and 5'-CCTGGCGAGGAGTTTCAATA-3'). Each sample was analyzed in triplicate and then differences in the expression of each gene were quantified using the ΔΔCt approach using the endogenous control.

Western blot analysis

Cells were lysed in RIPA lysis buffer [50 mM Tris-HCl pH 7.8, 150 mM NaCl, 2 mM EDTA, 1 % Triton X-100, 0.1 % SDS supplemented with protease inhibitors (Sigma, P8340)] then 25 or 50 µg of lysates were resolved on a 12% or 15% polyacrylamide gel in Running buffer (25 mM Tris base, 192 mM glycine and 0.1% SDS) at 60 V for 60 min and 120 V for another 60 min. Proteins were transferred onto Immuno-Blot PVDF 0.2 µm membranes (Bio-Rad, 162-0177) for 90 min at

90 V at 4°C in Transfer buffer (25 mM Tris base, 192 mM glycine, 0.037% SDS and 20% methanol). Membranes were subsequently incubated in blocking buffer for 1 h [TBS-T (20 mM Tris-HCl, pH 7.6, 137 mM NaCl, 0.1 %Tween 20) containing 5% skim milk powder] and incubated with primary antibodies in blocking buffer overnight at 4°C. The secondary horseradish peroxidase-coupled anti-rabbit (Sigma-Aldrich, A0545) and anti-mouse IgG antibodies (Sigma-Aldrich, A4416) were prepared in TBS-T. After 1 h incubation, the membrane was washed 3 times in TBS-T and incubated with the Pierce ECL western-blotting substrate (Pierce, 32106) according to the manufacturer's recommendations. All western blots were analyzed using the ChemiDoc XRS+ from Biorad. All western blot signals were quantified before saturation using the Image Lab 2.0 software provided with the ChemiDoc XRS+ according to the manufacturer's instructions.

For the HNE western-blotting, cells were lysed in HNE lysis buffer (50 mM Hepes, 150 mM NaCl, 1.5 mM MgCl, 1 mM EDTA, 1% glycerol, 1% NP40) supplemented with protease inhibitors (Sigma-Aldrich, P8340) and 50 mM N-Ethylmaleimide (NEM, Sigma-Aldrich, E3876). The samples were run the same day to avoid any freeze-thaw step. The goat anti-HNE antibody was purchased from Alpha Diagnostics (HNE-12S) and used at a 1:3000 dilution overnight in TBS-T supplemented with 5% Horse serum.

Cell proliferation assays

For the MTT assay, MDA-MB-436-shC and MDA-MB-436-sh2 cell lines were plated in 96-well plates (3,000 cells per well, 24 wells per cell line) and MTT assays were conducted every day over a 10-day period using 3-(4,5-dimethylthiazol-2-yl)-2,5-diphenyl tetrazolium bromide (MTT) (Sigma-Aldrich, M5655) as previously described.[13]

For the trypan blue exclusion assay, MDA-MB-436-shC and MDA-MB-436-sh2 cells were plated in 12-well plates (100,000 cells per well, 3 wells per cell line) and cells were counted every

day over a 4 d period. After discarding the culture medium, cells were incubated in 100 µl Trypsin-EDTA (Invitrogen, 25200-056) for 5 min at 37°C. After further addition of 200 µl of complete medium, cells were supplemented with 30 µl of trypan blue (0.04 % final concentration, Cellgro, 25-900-CI) and the viable cells density was then determined using a Malassez haemacytometer.

Colony formation assay

MDA-MB-436-shC and MDA-MB-436-sh2 cells were plated in 6-well plates (3,000 cells per well) and incubated in complete culture medium supplemented with 10% FBS, 100 µg/mL Penicillin/Streptomycin and 1 mM L-Glutamine at 37°C and 5% CO_2. After 12 d, the colonies formed were fixed 10 min. with 100% ethanol and stained for 10 min. with crystal violet (0.5% in 2% ethanol). Each well was then washed 3 times with distilled water and colonies were counted using the Vision-Capt software (Vilber Lourmat).

Cell invasion assay

Cell invasion was evaluated using modified Boyden chambers (6.5 mm diameter and 8 µm pore size, SPL Life Sciences). Boyden chambers were coated with 50 µg ECM gel from Engelbreth-Holm-Swarm murine sarcoma (Sigma-Aldrich, E1270) diluted in DMEM and incubated for 5 h at 37°C. 100,000 cells in 250 µl of serum-free DMEM were seeded into the upper chamber and 500 µl of complete culture medium were added in the lower compartment. After 24 h incubation in a 5% CO_2 incubator at 37°C, cells on the upper surface were removed using a swab and cells on the lower surface were fixed 5 min with absolute ethanol and stained with crystal violet (0.5% in 2% ethanol) for 10 min. The filters were then washed with distilled water and cells were counted using a light microscope at a high magnification (x400).

Cathepsins B and D activity assays

Cathepsin B and Cathepin D activities were quantified using the Cathepsin B Activity Assay Kit (Abnova, KA0766) and the Cathepsin D activity assay kit (Sigma, CS0800) following manufacturer's instructions. Briefly, cells were collected by scraping and centrifugation (1500 g for 5 min at 4°C), washed once with PBS before a second spin and then lysed using Cathepsin B cell lysis buffer (kit) or MES lysis buffer for Cathepsin D (20 mM MES pH 6.8, 20 mM NaCl, 1 mM $MgCl_2$, 2 mM EDTA, 10 mM NaH_2PO_4) supplemented with phosphatase (Sigma, P0044) and protease (Sigma, P8340) inhibitors. Lysates were then incubated for 30 min on ice, centrifuged at 15000 g for 5 min and supernatants were subjected to DC-Bradford assay (Bio-Rad, 500-0114).

For the Cathepsin B activity assay, 50 µg of cell lysate were combined with the Cathepsin B reaction buffer (kit) in a 96-well black plate with clear top and bottom. E64 (Sigma, E8640) was used for inhibition of Cathepsin B activity. After addition of a fluorogenic Cathepsin B substrate (kit), the plate was incubated for 2 h at 37°C before values were read in fluorescence units (FLU) which were then normalized to controls.

For the Cathepsin D activity assay, 30 µg of lysate per sample were used for activity readings with and without Pepstatin A (PepA, 2 mg/ml, Sigma, P5318) in a black 96-well plate with clear top and bottom. PepA values were subtracted from non-PepA values to determine Cathepsin D activity in fluorescence units (FLU) which were then normalized to control samples.

Mitochondrial bioenergetic measurements using the Seahorse XF-24 analyzer

To measure mitochondrial function in MDA-MB-436-shC and MDA-MB-436-sh2 cells, a Seahorse Bioscience XF24 extracellular flux analyzer was used. To allow comparison between experiments, data are expressed as the oxygen consumption rate (OCR) in pmol/min or the extracellular acidification rate (ECAR) in mpH/min, normalized to cell protein contents determined

by the DC-Bradford (Bio-Rad, 500-0114) method. The optimal seeding density of the cells needed to obtain measurable OCR and ECAR was established, and both ECAR and OCR show a proportional response with cell number (data not shown). For our experiments, a seeding density of 60,000 cells per well was selected to allow both increase and inhibition of OCR and ECAR. In our experiments, oligomycin, FCCP, and antimycin A concentrations were 1, 0.75, and 10 µM, respectively.

ATP assay

MDA-MB-436-shC and MDA-MB-436-sh2 cells were plated in 96-well plates (40,000 per well) and incubated for 24 h at 37°C. The intracellular ATP concentration was then assessed using the ATPlite kit from PerkinElmer (6016943) according to the manufacturer's recommendations. Briefly, culture medium was discarded and cells were incubated first for 5 min in the kit lysis buffer, then for further 5 min with the substrate solution, before being adapted to the dark for 10 min. Emitted luminescence was then measured using a Victor^{2}V PerkinElmer Wallac 1420 Multilabel Counter. The intracellular ATP amounts (in pmol) were calculated according to an ATP standard curve and normalized to the quantity of protein in each sample using a DC-Bradford assay (Bio-Rad, 500-0114).

GSH recycling assay

The quantification of GSH in our two cell lines was performed according to the protocol previously described.[62] Briefly, MDA-MB-436-shC and MDA-MB-436-sh2 cells were plated in 6-well plates (600,000 per well) and incubated for 24 h at 37°C. Culture medium was discarded and cells were washed twice in GSH wash buffer (10 µM DTPA, diethylenetriaminepentaacetic acid, in 1 X PBS, Sigma-Aldrich, D6518) before lysis in GSH wash buffer supplemented with 0.1% Triton X-100 for 10 min on ice. Collected cells were centrifuged at 12,000 g for 15 min and

supernatants were collected for GSH quantification. The reaction sample was composed of 10 µl sample, 60 µl DTNB [5,5′-dithiobis(2-nitrobenzoic acid), 10 mM, Sigma-Aldrich, D8130], 900 µl GSH wash buffer, 20 µl NAD(P)H (10 mM, Sigma-Aldrich, N1630) and 10 µl glutathione reductase (Sigma-Aldrich, G9297). The fluorescence was then measured at 412 nm and 37°C over a 4 min period using a Beckman Coulter DU-800 spectrophotometer and the rates of the reactions were expressed in dAbs/min. The GSH amounts (in pmol) were determined according to a GSH standard curve and normalized to the quantity of protein in each sample using a DC-Bradford assay (Bio-Rad, 500-0114).

TMRM staining

MDA-MB-436-shC and MDA-MB-436-sh2 cells were plated in 96-well plates (40,000 per well) and incubated for 24 h at 37°C. Cells were then incubated with TMRM (TetraMethylRhodamine Methyl ester perchlorate, 100 nM) in phenol-free complete medium for 45 min at 37°C before being washed twice with PBS. TMRM fluorescence was then measured at 590 nm using a Victor^{3}V PerkinElmer Wallac 1420 Multilabel Counter. The TMRM cell incorporation determined as arbitrary units of fluorescence was then normalized to the quantity of protein in each sample using a DC-Bradford assay (Bio-Rad, 500-0114).

mtDNA quantification

DNA was extracted from MDA-MB-436-shC and MDA-MB-436-sh2 cells. Quantitative real-time PCR was performed by using a SYBR Green master mix (Roche, 04673484001) and an ABI7500 Roche LightCycler. The primer sequences used for mtDNA were mtDNA-F (5'-CACCCAAGAACAGGGTTTGT-3') and mtDNA-R (5'-TGGCCATGGGTATGTTGTTAA-3'). The primer sequences for the nuclear DNA were 18S-F (5'-TAGAGGGACAAGTGGCGTTC-3') and 18S-R (5'-CGCTGAGCCAGTCAGTGT-3') and targeted the human nuclear 18S DNA. Cycling

conditions were as follows: 94°C for 15 s, followed by 40 cycles at 94°C for 15 s, 60°C for 1 min and 60°C for 1 min. The mtDNA copy number was normalized to the amplification of the 18S nuclear amplicon.

mtDNA damage assay

Mitochondrial DNA damage was evaluated by PCR method as described previously.[63] Briefly, total DNA was extracted and used as PCR sample. The primer sequences used for mtDNA long segment (16 kb) were mtLongF (5′-TGA GGC CAA ATA TCA TTC TGA GGG GC-3′) and mtLongR (5′-TTT CAT CAT GCG GAG ATG TTG GAT GG-3′). The primer sequences for mtDNA short (80 bp) segment were mtShortF (5′-ACCCAAGAACAGGGTTTGT-3′) and mtShortR (5′-TGGCCATGGGTATGTTGTTAA-3′). The mtDNA long and short segments were amplified using AccuPrime™ Taq DNA Polymerase High Fidelity kit (Life Tech Corp) and separated by agarose gel electrophoresis. The long PCR conditions were as follow: 94°C for 11 sec, followed by 27 cycles of denaturation at 94°C for 15 sec, 67°C for 12 min and a final extension at 72°C for 10 min. The short PCR conditions were as follow: 94°C for 5 sec, followed by 19 cycles at 94°C for 25 sec, 60°C for 45 sec, 72°C for 1 min, and a final extension at 72°C for 10 min. The gels were stained with ethidium bromide and visualized with Alpha Imager. Densitometry analysis was performed using Image J software. Lesion frequency per 16 kb of mtDNA was calculated using as described previously. [64, 65]

Mitochondria staining

Cells were plated in four-well Labtek chambers (Nunc, 155-383) at a concentration of 100,000 cells per well and incubated at 37°C overnight. Cells were stained in fresh complete medium with 50 nM Mitotracker® red CMXRos (Invitrogen, M7512). Living cells were then examined using a fluorescence laser scanning Zeiss LSM 710 confocal microscope (UAB microscopy core,

Birmingham, AL). Images were captured using the Zen 2008 software. All figures were assembled using Adobe Photoshop CS2 and Adobe Illustrator CS software.

LAMP1 immunostaining

Cells cultured for 24 h on coverslips in 24-well plates were washed with PBS and fixed with 4% paraformaldehyde in PBS for 15 min at room temperature. Cells were then permeabilized with 0.2% Triton-X100 in PBS for 5 min, washed thrice for 5 min with PBS, blocked with 5% BSA in PBS for 30 min, incubated with a monoclonal anti-mouse LAMP1 (Abcam, Ab25630, 1:100) overnight at 4°C and finally with an Alexa Fluor 555 goat anti-mouse (Life technologies, A-21422, 1:800) for 1 h. After being washed thrice for 5 min, the cells were analyzed using a confocal microscope.

Mitophagy analysis

Cells (280,000) were plated in Lab-TekTMII chambers (Nunc, 155380) for 24 h and and incubated at 37°C overnight. Cells were stained in fresh complete medium with 50 nM Mitotracker® red CMXRos (Invitrogen, M7512) and 100 nM Lysotracker® green (Invitrogen, L-7526) for 45 min in the presence or absence of 10 μM FCCP (Sigma, C2920) for 45 min. Live cells were then analyzed using a Zeiss LSM 710 confocal microscope and the Zen 2008 software. All figures were assembled using Adobe Photoshop CS2 and Adobe Illustrator CS softwares. For mitophagy measurements, red and green pixel intensity overlay was conducted using ImageJ software (Coloc 2) and the Pearson's coefficient.

Flow cytometry

Cells were plated in 6-well plates at a concentration of 600,000 cells per well and incubated at 37°C overnight. Cells were stained in fresh complete medium with 50 nM Mitotracker® red

CMXRos for 45 min. After two PBS washes, cells were trypsinized and resuspended in 200 µl complete medium before being harvested at 5,000 g for 5 min and resuspended in 500 µl PBS. Cells (10,000 events) were then examined using a LSR II Becton Dickinson flow cytometer (UAB Flow Cytometry Core, Birmingham, AL). Data were acquired and analyzed using the Becton Dickinson FACScan Flow Cytometer software.

Statistical analyses

Statistical analyses were carried out using a Student's t test. Data are expressed as the mean ± SEM.

Acknowledgement

Michaël Boyer-Guittaut would like to thank his colleagues from the EA3922 team, Mr Jacques Bahi, President of the Université of Franche-Comté, Mr Abderrazzak Kadmiri, Director of UFR-ST of the Université of Franche-Comté and the Université of Franche-Comté for their support during this research project performed at the University of Alabama at Birmingham, USA. Laura Poillet is supported by a fellowship of the Région de Franche-Comté. The authors acknowledge funding from the following sources: Dr. Jianhua Zhang was supported by NIHR01-NS064090 and a VA merit award. Flow cytometry was supported by RDCC-APCC core (NIH P30 grant #P30 AR48311). The authors would like to thank Enid F. Keyser (UAB Flow cytometry core, Birmingham, AL) for her technical help using the LSR-II Becton Dickinson flow cytometer. Authors are grateful to Jianhua Zhang's and Victor M. Darley-Usmar's laboratory members for their technical help, advice and critical reviewing of this manuscript.

Financial disclosure

VDU is a member of the Seahorse Biosciences Scientific Advisory Board.

References

1. Pellerin I, Vuillermoz C, Jouvenot M, Ordener C, Royez M, Adessi GL. Identification and characterization of an early estrogen-regulated RNA in cultured guinea-pig endometrial cells. Molecular and cellular endocrinology 1993; 90:R17-21.
2. Chakrama FZ, Seguin-Py S, Le Grand JN, Fraichard A, Delage-Mourroux R, Despouy G, et al. GABARAPL1 (GEC1) associates with autophagic vesicles. Autophagy 2010; 6.
3. Wang H, Bedford FK, Brandon NJ, Moss SJ, Olsen RW. GABA(A)-receptor-associated protein links GABA(A) receptors and the cytoskeleton. Nature 1999; 397:69-72.
4. Shpilka T, Weidberg H, Pietrokovski S, Elazar Z. Atg8: an autophagy-related ubiquitin-like protein family. Genome biology 2011; 12:226.
5. Mansuy V, Boireau W, Fraichard A, Schlick JL, Jouvenot M, Delage-Mourroux R. GEC1, a protein related to GABARAP, interacts with tubulin and GABA(A) receptor. Biochem Biophys Res Commun 2004; 325:639-48.
6. Chen C, Li JG, Chen Y, Huang P, Wang Y, Liu-Chen LY. GEC1 interacts with the kappa opioid receptor and enhances expression of the receptor. J Biol Chem 2006; 281:7983-93.
7. Mansuy-Schlick V, Tolle F, Delage-Mourroux R, Fraichard A, Risold PY, Jouvenot M. Specific distribution of gabarap, gec1/gabarap Like 1, gate16/gabarap Like 2, lc3 messenger RNAs in rat brain areas by quantitative real-time PCR. Brain research 2006; 1073-1074:83-7.
8. Tolle F, Risold PY, Mansuy-Schlick V, Rossi E, Boyer-Guittaut M, Fraichard A, et al. Specific regional distribution of gec1 mRNAs in adult rat central nervous system. Brain research 2008; 1210:103-15.
9. Le Grand JN, Bon K, Fraichard A, Zhang J, Jouvenot M, Risold PY, et al. Specific distribution of the autophagic protein GABARAPL1/GEC1 in the developing and adult mouse brain and identification of neuronal populations expressing GABARAPL1/GEC1. PLoS One 2013; 8:e63133.
10. Sengupta A, Molkentin JD, Yutzey KE. FoxO transcription factors promote autophagy in cardiomyocytes. The Journal of biological chemistry 2009; 284:28319-31.
11. Jamart C, Benoit N, Raymackers JM, Kim HJ, Kim CK, Francaux M. Autophagy-related and autophagy-regulatory genes are induced in human muscle after ultraendurance exercise. European journal of applied physiology 2012; 112:3173-7.
12. Nemos C, Mansuy V, Vernier-Magnin S, Fraichard A, Jouvenot M, Delage-Mourroux R. Expression of gec1/GABARAPL1 versus GABARAP mRNAs in human: predominance of gec1/GABARAPL1 in the central nervous system. Brain Res Mol Brain Res 2003; 119:216-9.
13. Berthier A, Seguin S, Sasco AJ, Bobin JY, De Laroche G, Datchary J, et al. High expression of gabarapl1 is associated with a better outcome for patients with lymph node-positive breast cancer. Br J Cancer 2010; 102:1024-31.
14. De Palma C, Morisi F, Cheli S, Pambianco S, Cappello V, Vezzoli M, et al. Autophagy as a new therapeutic target in Duchenne muscular dystrophy. Cell death & disease 2012; 3:e418.
15. von Walden F, Jakobsson F, Edstrom L, Nader GA. Altered autophagy gene expression and persistent atrophy suggest impaired remodeling in chronic hemiplegic human skeletal muscle. Muscle & nerve 2012; 46:785-92.
16. Simunovic F, Yi M, Wang Y, Macey L, Brown LT, Krichevsky AM, et al. Gene expression profiling of substantia nigra dopamine neurons: further insights into Parkinson's disease pathology. Brain : a journal of neurology 2009; 132:1795-809.
17. Lee J, Giordano S, Zhang J. Autophagy, mitochondria and oxidative stress: cross-talk and redox signalling. The Biochemical journal 2012; 441:523-40.
18. Hill BG, Benavides GA, Lancaster JR, Jr., Ballinger S, Dell'Italia L, Jianhua Z, et al. Integration of cellular bioenergetics with mitochondrial quality control and autophagy. Biological chemistry 2012; 393:1485-512.

19. Mitchell T, Chacko B, Ballinger SW, Bailey SM, Zhang J, Darley-Usmar V. Convergent mechanisms for dysregulation of mitochondrial quality control in metabolic disease: implications for mitochondrial therapeutics. Biochem Soc Trans 2013; 41:127-33.
20. Zhang J. Autophagy and Mitophagy in Cellular Damage Control. Redox Biol 2013; 1:19-23.
21. Dodson M, Darley-Usmar V, Zhang J. Cellular metabolic and autophagic pathways: Traffic control by redox signaling. Free radical biology & medicine 2013; 63:207-21.
22. Benbrook DM, Long A. Integration of autophagy, proteasomal degradation, unfolded protein response and apoptosis. Experimental oncology 2012; 34:286-97.
23. Yang Z, Klionsky DJ. An overview of the molecular mechanism of autophagy. Current topics in microbiology and immunology 2009; 335:1-32.
24. Hill BG, Benavides GA, Lancaster JR, Ballinger S, Dell'italia L, Zhang J, et al. Integration of cellular bioenergetics with mitochondrial quality control and autophagy. Biological chemistry 2012.
25. Higdon A, Diers AR, Oh JY, Landar A, Darley-Usmar VM. Cell signalling by reactive lipid species: new concepts and molecular mechanisms. The Biochemical journal 2012; 442:453-64.
26. Weidberg H, Shvets E, Shpilka T, Shimron F, Shinder V, Elazar Z. LC3 and GATE-16/GABARAP subfamilies are both essential yet act differently in autophagosome biogenesis. EMBO J 2010; 29:1792-802.
27. Cann GM, Guignabert C, Ying L, Deshpande N, Bekker JM, Wang L, et al. Developmental expression of LC3alpha and beta: absence of fibronectin or autophagy phenotype in LC3beta knockout mice. Developmental dynamics : an official publication of the American Association of Anatomists 2008; 237:187-95.
28. O'Sullivan GA, Kneussel M, Elazar Z, Betz H. GABARAP is not essential for GABA receptor targeting to the synapse. The European journal of neuroscience 2005; 22:2644-8.
29. Chen ZH, Lam HC, Jin Y, Kim HP, Cao J, Lee SJ, et al. Autophagy protein microtubule-associated protein 1 light chain-3B (LC3B) activates extrinsic apoptosis during cigarette smoke-induced emphysema. Proceedings of the National Academy of Sciences of the United States of America 2010; 107:18880-5.
30. Shaid S, Brandts CH, Serve H, Dikic I. Ubiquitination and selective autophagy. Cell death and differentiation 2013; 20:21-30.
31. Novak I, Kirkin V, McEwan DG, Zhang J, Wild P, Rozenknop A, et al. Nix is a selective autophagy receptor for mitochondrial clearance. EMBO reports 2010; 11:45-51.
32. Jiang S, Heller B, Tagliabracci VS, Zhai L, Irimia JM, DePaoli-Roach AA, et al. Starch binding domain-containing protein 1/genethonin 1 is a novel participant in glycogen metabolism. The Journal of biological chemistry 2010; 285:34960-71.
33. Jiang S, Wells CD, Roach PJ. Starch-binding domain-containing protein 1 (Stbd1) and glycogen metabolism: Identification of the Atg8 family interacting motif (AIM) in Stbd1 required for interaction with GABARAPL1. Biochemical and biophysical research communications 2011; 413:420-5.
34. Zhang Y, Wang F, Han L, Wu Y, Li S, Yang X, et al. GABARAPL1 negatively regulates Wnt/beta-catenin signaling by mediating Dvl2 degradation through the autophagy pathway. Cell Physiol Biochem 2011; 27:503-12.
35. Debnath J. The multifaceted roles of autophagy in tumors-implications for breast cancer. Journal of mammary gland biology and neoplasia 2011; 16:173-87.
36. Arduino DM, Esteves AR, Cortes L, Silva DF, Patel B, Grazina M, et al. Mitochondrial metabolism in Parkinson's disease impairs quality control autophagy by hampering microtubule-dependent traffic. Human molecular genetics 2012; 21:4680-702.
37. Ishii T, Warabi E, Siow RC, Mann GE. Sequestosome1/p62: A regulator of redox-sensitive voltage-activated potassium channels, arterial remodeling, inflammation, and neurite outgrowth. Free radical biology & medicine 2013; 65C:102-16.

38. Liang Q, Benavides GA, Vasilopoulos A, Gius D, Darley-Usmar V, Zhang J. Bioenergetic and autophagic control by Sirt3 in response to nutrient deprivation in mouse embryonic fibroblasts. The Biochemical journal 2013.
39. Kurzawa-Akanbi M, Hanson PS, Blain PG, Lett DJ, McKeith IG, Chinnery PF, et al. Glucocerebrosidase mutations alter the endoplasmic reticulum and lysosomes in Lewy body disease. J Neurochem 2012; 123:298-309.
40. Dranka BP, Benavides GA, Diers AR, Giordano S, Zelickson BR, Reily C, et al. Assessing bioenergetic function in response to oxidative stress by metabolic profiling. Free radical biology & medicine 2011; 51:1621-35.
41. Schneider L, Giordano S, Zelickson BR, M SJ, G AB, Ouyang X, et al. Differentiation of SH-SY5Y cells to a neuronal phenotype changes cellular bioenergetics and the response to oxidative stress. Free radical biology & medicine 2011; 51:2007-17.
42. Meirhaeghe A, Crowley V, Lenaghan C, Lelliott C, Green K, Stewart A, et al. Characterization of the human, mouse and rat PGC1 beta (peroxisome-proliferator-activated receptor-gamma co-activator 1 beta) gene in vitro and in vivo. The Biochemical journal 2003; 373:155-65.
43. Shoshan-Barmatz V, Mizrachi D. VDAC1: from structure to cancer therapy. Frontiers in oncology 2012; 2:164.
44. Chen H, Chan DC. Physiological functions of mitochondrial fusion. Annals of the New York Academy of Sciences 2010; 1201:21-5.
45. Blackstone C, Chang CR. Mitochondria unite to survive. Nature cell biology 2011; 13:521-2.
46. Ashrafi G, Schwarz TL. The pathways of mitophagy for quality control and clearance of mitochondria. Cell death and differentiation 2013; 20:31-42.
47. Sansbury BE, Jones SP, Riggs DW, Darley-Usmar VM, Hill BG. Bioenergetic function in cardiovascular cells: the importance of the reserve capacity and its biological regulation. Chemico-biological interactions 2011; 191:288-95.
48. Guo J, Prokai-Tatrai K, Nguyen V, Rauniyar N, Ughy B, Prokai L. Protein targets for carbonylation by 4-hydroxy-2-nonenal in rat liver mitochondria. Journal of proteomics 2011; 74:2370-9.
49. Fritz KS, Galligan JJ, Smathers RL, Roede JR, Shearn CT, Reigan P, et al. 4-Hydroxynonenal inhibits SIRT3 via thiol-specific modification. Chemical research in toxicology 2011; 24:651-62.
50. Falletti O, Douki T. Low glutathione level favors formation of DNA adducts to 4-hydroxy-2(E)-nonenal, a major lipid peroxidation product. Chemical research in toxicology 2008; 21:2097-105.
51. Klebig C, Seitz S, Arnold W, Deutschmann N, Pacyna-Gengelbach M, Scherneck S, et al. Characterization of {gamma}-aminobutyric acid type A receptor-associated protein, a novel tumor suppressor, showing reduced expression in breast cancer. Cancer research 2005; 65:394-400.
52. Lock R, Roy S, Kenific CM, Su JS, Salas E, Ronen SM, et al. Autophagy facilitates glycolysis during Ras-mediated oncogenic transformation. Molecular biology of the cell 2011; 22:165-78.
53. Carew JS, Kelly KR, Nawrocki ST. Autophagy as a target for cancer therapy: new developments. Cancer management and research 2012; 4:357-65.
54. Sarkar S, Davies JE, Huang Z, Tunnacliffe A, Rubinsztein DC. Trehalose, a novel mTOR-independent autophagy enhancer, accelerates the clearance of mutant huntingtin and alpha-synuclein. The Journal of biological chemistry 2007; 282:5641-52.
55. Dehay B, Bove J, Rodriguez-Muela N, Perier C, Recasens A, Boya P, et al. Pathogenic lysosomal depletion in Parkinson's disease. J Neurosci 2010; 30:12535-44.
56. Chauhan S, Goodwin JG, Manyam G, Wang J, Kamat AM, Boyd DD. ZKSCAN3 is a master transcriptional repressor of autophagy. Mol Cell 2013; 50:16-28.
57. Kunzli N. Happy birthday MPH (Master of Public Health): it's time for the party--a reality check and a cure. Soz Praventivmed 2002; 47:279-80.
58. Ohri SS, Vashishta A, Proctor M, Fusek M, Vetvicka V. The propeptide of cathepsin D increases proliferation, invasion and metastasis of breast cancer cells. Int J Oncol 2008; 32:491-8.

59. Chen QY, Shi JG, Yao QH, Jiao DM, Wang YY, Hu HZ, et al. Lysosomal membrane permeabilization is involved in curcumin-induced apoptosis of A549 lung carcinoma cells. Mol Cell Biochem 2012; 359:389-98.
60. Rudd LP, Kabler SL, Morrow CS, Townsend AJ. Enhanced glutathione depletion, protein adduct formation, and cytotoxicity following exposure to 4-hydroxy-2-nonenal (HNE) in cells expressing human multidrug resistance protein-1 (MRP1) together with human glutathione S-transferase-M1 (GSTM1). Chemico-biological interactions 2011; 194:113-9.
61. Dickinson DA, Levonen AL, Moellering DR, Arnold EK, Zhang H, Darley-Usmar VM, et al. Human glutamate cysteine ligase gene regulation through the electrophile response element. Free Radic Biol Med 2004; 37:1152-9.
62. Tietze F. Enzymic method for quantitative determination of nanogram amounts of total and oxidized glutathione: applications to mammalian blood and other tissues. Analytical biochemistry 1969; 27:502-22.
63. Knight-Lozano CA, Young CG, Burow DL, Hu ZY, Uyeminami D, Pinkerton KE, et al. Cigarette smoke exposure and hypercholesterolemia increase mitochondrial damage in cardiovascular tissues. Circulation 2002; 105:849-54.
64. Westbrook DG, Anderson PG, Pinkerton KE, Ballinger SW. Perinatal tobacco smoke exposure increases vascular oxidative stress and mitochondrial damage in non-human primates. Cardiovasc Toxicol 2010; 10:216-26.
65. Mitchell T, Johnson MS, Ouyang X, Chacko BK, Mitra K, Lei X, et al. Dysfunctional mitochondrial bioenergetics and oxidative stress in Akita+/Ins2-derived beta-cells. Am J Physiol Endocrinol Metab 2013.

Figure legends

Figure 1: GABARAPL1 mRNA and protein expression are significantly decreased in the MDA-MB-436-sh2 clone.

(**A**) *GABARAPL1*, *GABARAP* and *LC3B* mRNA expression was analyzed by qRT-PCR in the different MDA-MB-436 stable cell lines. The different stable cell lines, expressing one of the five shRNAs directed against the *GABARAPL1* gene (sh1 to sh5), were compared to the stable MDA-MB-436 cell line expressing a control shRNA (shC). *: $p<0.05$, vs shC (n=3). (**B**) GABARAPL1 expression levels in the MDA-MB-436 stable cell lines were determined by western blotting. Total proteins (40 µg) were separated on a 15% SDS-PAGE and immunoblotted using anti-GABARAPL1 (Proteintech) and anti-Actin antibodies and the ECL Plus reagent. A representative experiment of 3 performed is shown. Rat whole brain extract (WBE) was used as a positive control of GABARAPL1 expression. (**C**) Quantification of the signals observed on the western blot in B. ★: $p<0.05$, vs shC (n=3).

Figure 2: GABARAPL1 knock-down promotes cell growth, colony formation and invasion.

(**A**) MDA-MB-436-shC, sh2 and sh5 cell growth was determined using a MTT assay over an 8-day period. All data were normalized to the number of cells at Day 1 for each cell line. ★: $p<0.05$, vs shC (n=24). (**B**) MDA-MB-436-shC and sh2 cells (3,000 in 6-well plates) were grown for a period of 12 days then fixed and stained with crystal violet. The number of colonies was then determined using the Vision-Capt software (Vilber Lourmat). A representative experiment of 3 performed is shown. ★: $p<0.05$, vs shC (n=3). (**C**) MDA-MB-436-shC and sh2 cells were grown in modified Boyden chambers coated with ECM gel. After a 24 h incubation at 37°C, cells in the upper chamber were swabbed while cells in the lower chamber were fixed, stained with crystal violet and counted using a light microscope at a high magnification (x400). A representative

experiment of 3 performed is shown. ★: p<0.05, vs shC (n=3).

Figure 3: GABARAPL1 knock-down inhibits autophagic flux without changing MTOR signaling.
(**A**) MDA-MB436-shC, sh2 and sh5 cells were cultured for 5 h in the presence (lanes 4-6 and 10-12) or absence (lanes 1-3 and 7-9) of the lysosome inhibitor chloroquine (40 μM). Total proteins (25 μg) were separated on 12% SDS-PAGE followed by immunoblotting with anti-LC3 and anti-Actin antibodies and the ECL Plus reagent. A representative experiment of 3 performed is shown. (**B**) The autophagy flux was determined as the levels of LC3-II in the presence of chloroquine divided by the levels of LC3-II in absence of chloroquine. ★: p<0.05, vs shC (n=3). (**C**) MDA-MB436-shC and sh2 cells were cultured for 24 h at 37°C and 5% CO_2 then total proteins (25 μg) were separated on 12% SDS-PAGE followed by immunoblotting with anti-phospho-MTOR, anti-MTOR, anti-phospho-p70S6K, anti-p70S6K, and anti-ACTIN antibodies and the ECL Plus reagent. A representative experiment of 3 performed is shown. ★: p<0.05, vs shC (n=3). (**D**) Quantification of the signals observed on the western blot in C (n=3).

Figure 4: GABARAPL1 knock-down leads to increased SQSTM1 and BECN1 proteins.
(**A**) MDA-MB436-shC, sh2 and sh5 cells were cultured for 24 h at 37°C and 5% CO_2 then total proteins (25 μg) were separated on 12% SDS-PAGE followed by immunoblotting with anti-BECN1, anti-SQSTM1 and anti-ACTIN antibodies and the ECL Plus reagent. A representative experiment of 3 performed is shown. (**B**) Quantification of the signals observed on the western blot in A. ★: p<0.05, vs shC (n=3). (**C**) *GABARAPL1*, *GABARAP, LC3B, BECN1,* and *SQSTM1* mRNA expression was analyzed by qRT-PCR in the MDA-MB436-shC and sh2 cells. ★: p<0.05, vs shC (n=3). (**D**) MDA-MB436-shC and sh2 cells were co-transfected with the vectors expressing HA-SQSTM1 and pEGFP-N1 (ratio 10:1). Forty eight hours after transfection, total

proteins (25 µg) were separated on 12% SDS-PAGE, followed by immunoblotting with anti-HA, anti-GFP and anti-ACTIN antibodies and the ECL Plus reagent. A representative experiment of 3 performed is shown. (**E**) Quantification of the signals observed on the western blot in D. ★: $p<0.05$, vs shC (n=3).

Figure 5: GABARAPL1 knock-down leads to decreased LAMP1 protein levels and immunocytochemistry staining.

(**A**) MDA-MB436-shC, sh2 and sh5 cells were cultured for 24 h at 37°C and 5% CO_2 then total proteins (25 µg) were separated on 12% SDS-PAGE followed by immunoblotting with anti-LAMP1 antibodies and the ECL Plus reagent. A representative experiment of 3 performed is shown. (**B**) Quantification of the signals observed on the western blot in A. ★: $p<0.05$, vs shC (n=3). (**C**) *GABARAPL1* and *LAMP1* mRNA expression was analyzed by qRT-PCR in the MDA-MB436-shC and sh2 cells. ★: $p<0.05$, vs shC. (**D**) MDA-MB436-shC, sh2 and sh5 cells were cultured for 24 h at 37°C and 5% CO_2, fixed, permeabilized, blocked with 5% BSA, incubated with a monoclonal anti-mouse LAMP1 overnight at 4°C and then with an Alexa Fluor 555 goat anti-mouse for 1 h. The cells were then analyzed using a confocal microscope. Each picture is representative of a typical cell staining observed in 10 fields chosen at random.

Figure 6: GABARAPL1 knock-down increases TMRM and Mitotracker red staining.

(**A**) TMRM staining (AU, arbitrary units) normalized to total protein. MDA-MB436-shC and sh2 cells (40,000) were cultured in 96-well plates for 24 h at 37°C and 5% CO_2. Cells were then incubated with 100 nM TMRM for 45 min before being washed with PBS. TMRM fluorescence was measured at 590 nm using a Victor^{3}V PerkinElmer Wallac 1420 Multilabel Counter. FCCP as a control decreased mitochondrial membrane potential to ~ 750 in both shC and sh2 cells. ★:

p<0.05, vs shC (n=3). #: p<0.05, vs without FCCP (n=3). (**B**) Mitotracker red fluorescence values (AU) for the two cell lines shC and sh2. Cells (600,000) were cultured in 6-well plates for 24 h at 37°C and 5% CO_2, stained with 50 nM mitotracker red for 45 min at 37°C, trypsinized, washed with PBS and resuspended in 500 µl PBS. Intracellular fluorescence was then assessed using the LSR-II Becton Dickinson flow cytometer. ★: p<0.05, vs shC (n=3). (**C**) MDA-MB436-shC and sh5 cells (100,000) were cultured in Labtek 4-well plates for 24 h at 37°C and 5% CO_2, stained with 50 nM Mitotracker red for 45 min at 37°C and washed with PBS. Mitochondria were imaged using the Zeiss LSM 710 confocal microscope and the Zen 2008 software. Mitotracker intensity was quantified by Image J for 25 cells for each cell line in 5 different fields of view chosen at random. ★: p<0.05, vs shC. (**D**) MDA-MB436-shC and sh2 cells (100,000) were cultured in Labtek 4-well plates for 24 h at 37°C and 5% CO_2, stained with 50 nM Mitotracker red for 45 min at 37°C and washed with PBS. Similarly, MDA-MB436-shC and sh5 cells (100,000) were cultured, stained with Mitotracker red and imaged. The pictures were taken with the Zeiss LSM 710 confocal microscope.

Figure 7: GABARAPL1 knock-down increases basal and proton leak Oxygen Consumption Rate (OCR), increases intracellular ATP levels, and decreases basal and maximal Respiratory Control Ratio (RCR).

MDA-MB436-shC and sh2 cells (60,000) were cultured for 24 h in 24-well XF24 Seahorse Biosciences V7 microplates and then bioenergetic function was assessed using the Seahorse XF24 analyzer. Both OCR and ECAR were measured. The ATP synthase inhibitor oligomycin (O; 1 µM), uncoupler FCCP (F; 0.75 µM), and complex III inhibitor antimycin A (A; 10 µM) were injected at the indicated times to determine different parameters of mitochondrial function. (**A**) Pictures showing similar confluency of the shC and sh2 cells before the start of the Seahorse

analysis. (**B**) OCR values shown as pmol O_2/min/µg protein. (**C**) Histogram showing the comparison of basal, ATP-linked, proton leak-linked, maximal, and non-mitochondrial OCR of shC and sh2 cells. Non-mitochondrial OCR was determined as the OCR after antimycin A treatment. Basal OCR was determined as OCR before oligomycin minus OCR after antimycin A. ATP-linked OCR was determined as OCR before oligomycin minus OCR after oligomycin. Proton leak was determined as basal OCR minus ATP-linked OCR. Maximal OCR was determined as the OCR after FCCP minus non-mitochondrial OCR. Reserve capacity was defined as the difference between maximal OCR after FCCP minus basal OCR. ★: $p<0.05$, vs shC (n=4). (**D**) ExtraCellular Acidification Rate (ECAR) values were plotted as mpH/min/µg protein for shC and sh2 cells (n=4). (**E**) Histogram showing the comparison of State apparent, RCR basal and RCR maximal of shC and sh2 cells. State apparent was determined as the value corresponding to the following formula: 4-[(Basal-Oligo)/(Basal-FCCP)]. RCR basal was determined as the value corresponding to the following formula: (Basal-AntiA)/(Oligo-AntiA). RCR maximal was determined as the value corresponding to the following formula: (FCCP-AntiA)/(Oligo-AntiA). ★: $p<0.05$, vs shC (n=4). (**F**) Histogram showing intracellular ATP values (pmoles/µg protein) for shC and sh2 cells. MDA-MB436-shC and sh2 cells (40,000) were cultured in 96-well plates for 24 h at 37°C and 5% CO_2. The intracellular ATP concentration was then determined using the ATPlite kit from PerkinElmer according to the manufacturer's instructions. Luminescence was measured using a Victor^{2}V PerkinElmer Wallac 1420 Multilabel Counter. ★: $p<0.05$, vs shC (n=3).

Figure 8: GABARAPL1 knock-down increases mitochondria number, and mtDNA damage.

(**A**) MDA-MB436-shC and sh2 cells were cultured for 24 h at 37°C and 5% CO_2. Cells were then lysed in the presence of protease and phosphatase inhibitors and total proteins (25 µg) were separated on 12% SDS-PAGE followed by immunoblotting with anti-PPARGC1A, anti-DNML1,

anti-MFN1, anti-VDAC1, anti-PARKIN, anti-PINK1 and anti-ACTIN antibodies and the ECL Plus reagent. A representative experiment of 3 performed is shown. (**B**) Quantification of the signals on the western blot in A. ★: p<0.05, vs shC (n=3). (**C**) MDA-MB436-shC and sh2 cells (600,000) were cultured in 6-well plates for 24 h at 37°C and 5% CO_2. Cells were washed with PBS and kept frozen at -80°C until purification of total DNA. Specific genomic and mitochondrial DNA sequences were amplified by quantitative real-time PCR. The data are presented as the ratio of mitochondrial versus genomic DNA and normalized to the control cell line, shC. ★: p<0.05, vs shC (n=3). (**D**) MDA-MB436-shC and sh2 cells (600,000) were cultured in 6-well plates for 24 h at 37°C and 5% CO_2. Cells were washed with PBS and kept frozen at -80°C until purification of total DNA. Specific long and short mitochondrial DNA sequences were amplified by PCR. The data were calculated from the levels of long mitochondrial PCR product versus levels of short mitochondrial PCR product as described in Materials and Methods, and normalized to shC. ★: p<0.05, vs shC (n=3).

Figure 9: GABARAPL1 knock-down enhances cell survival in response to HNE, inhibits autophagic flux in response to HNE, and increases intracellular HNE-protein adducts and glutathione (GSH) concentration.

(**A**) MDA-MB436-shC and sh2 cells were grown for 16 h in the presence of HNE (0, 5, 15 or 30 µM). Cells were then trypsinized and counted in the presence of trypan blue. The values were normalized to the number of cells determined in the control samples for each cell line. ★: p<0.05, vs shC (n=3). (**B**) MDA-MB436-shC and sh2 cells were cultured for 16 h in the presence of HNE (30 µM). Cells were then lysed and total proteins (25 µg) were separated on 12% SDS-PAGE followed by immunoblotting with anti-LC3 and anti-ACTIN antibodies and the ECL Plus reagent. A representative experiment of 3 performed is shown. (**C**) Quantification of the LC3-II signals

observed in the western blots shown in B. HNE-induced changes of LC3-II levels were determined as the levels of LC3-II in response to HNE divided by the levels of LC3-II without HNE. ★: $p<0.05$, vs shC (n=3), #: $p<0.05$, vs untreated cells (n=3). (**D**) MDA-MB436-shC and sh2 cells were cultured for 16 h in the presence of HNE (30 µM). Cells were then lysed in HNE lysis buffer containing 10 mM NEM (N-ethylmaleimide) and total proteins (25 µg) were separated on 12% SDS-PAGE followed by immunoblotting with anti-4-HNE and anti-ACTIN antibodies and the ECL Plus reagent. (**E**) Quantification of the signals observed in the western blot in D. ★: $p<0.05$, vs shC (n=3), #: $p<0.05$, vs untreated cells (n=3). (**F**) Total cellular GSH was determined using the GSH recycling assay, as described in the material and methods, using a Beckman Coulter DU-800 spectrophotometer, after shC and sh2 cells (600,000) were cultured in 6-well plates for 24 h at 37°C. ★: $p<0.05$, vs shC (n=3).

Figure 10: GABARAPL1 function in breast cancer cells.

Our studies indicate that GABARAPL1 plays an important role in autophagic flux, mitochondrial homeostasis, metabolic programming and control of cell proliferation in breast cancer MDA-MB-436 cells. *GABARAPL1* knock-down induces a disruption of the autophagosome-lysosome pathway leading to a decrease of lysosome number and accumulation of damaged mitochondria, increased mitochondrial biogenesis and number, and increased mitochondrial respiration, mitochondrial membrane potential, mitochondrial proteins and mtDNA damage. This is further evidenced by an increase of HNE-protein adducts, increased antioxidant response, and increased ATP levels. The increase of mitochondrial number, cellular glutathione, and cellular ATP may contribute to resistance to cell death and increased proliferation.

Figure 1

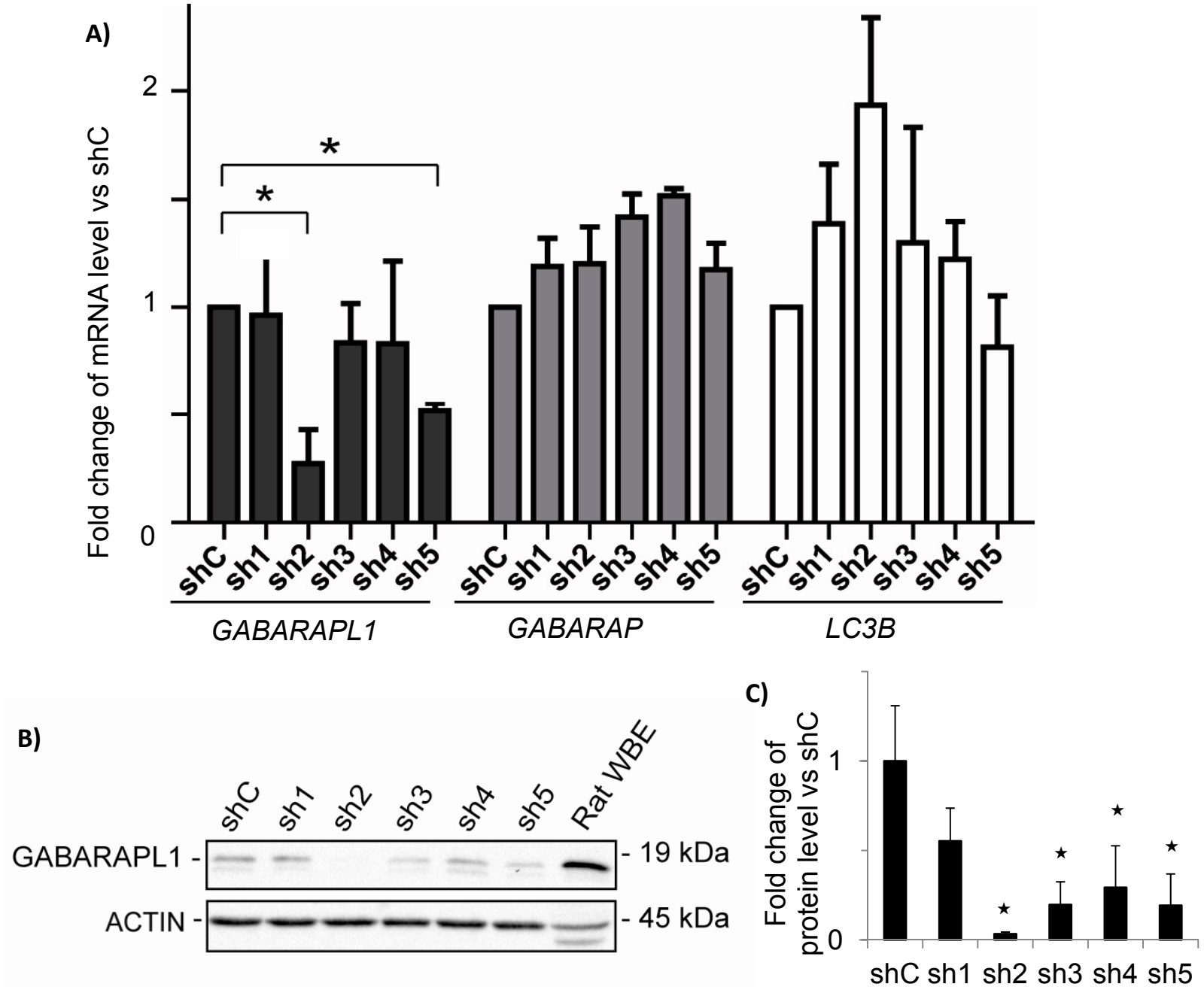
A)
Fold change of mRNA level vs shC
2
1
0
*
*
shC sh1 sh2 sh3 sh4 sh5
shC sh1 sh2 sh3 sh4 sh5
shC sh1 sh2 sh3 sh4 sh5
GABARAPL1
GABARAP
LC3B
B)
shC sh1 sh2 sh3 sh4 sh5 Rat WBE
GABARAPL1 -
- 19 kDa
ACTIN -
- 45 kDa
C)
Fold change of protein level vs shC
1
0
shC sh1 sh2 sh3 sh4 sh5

Figure 2

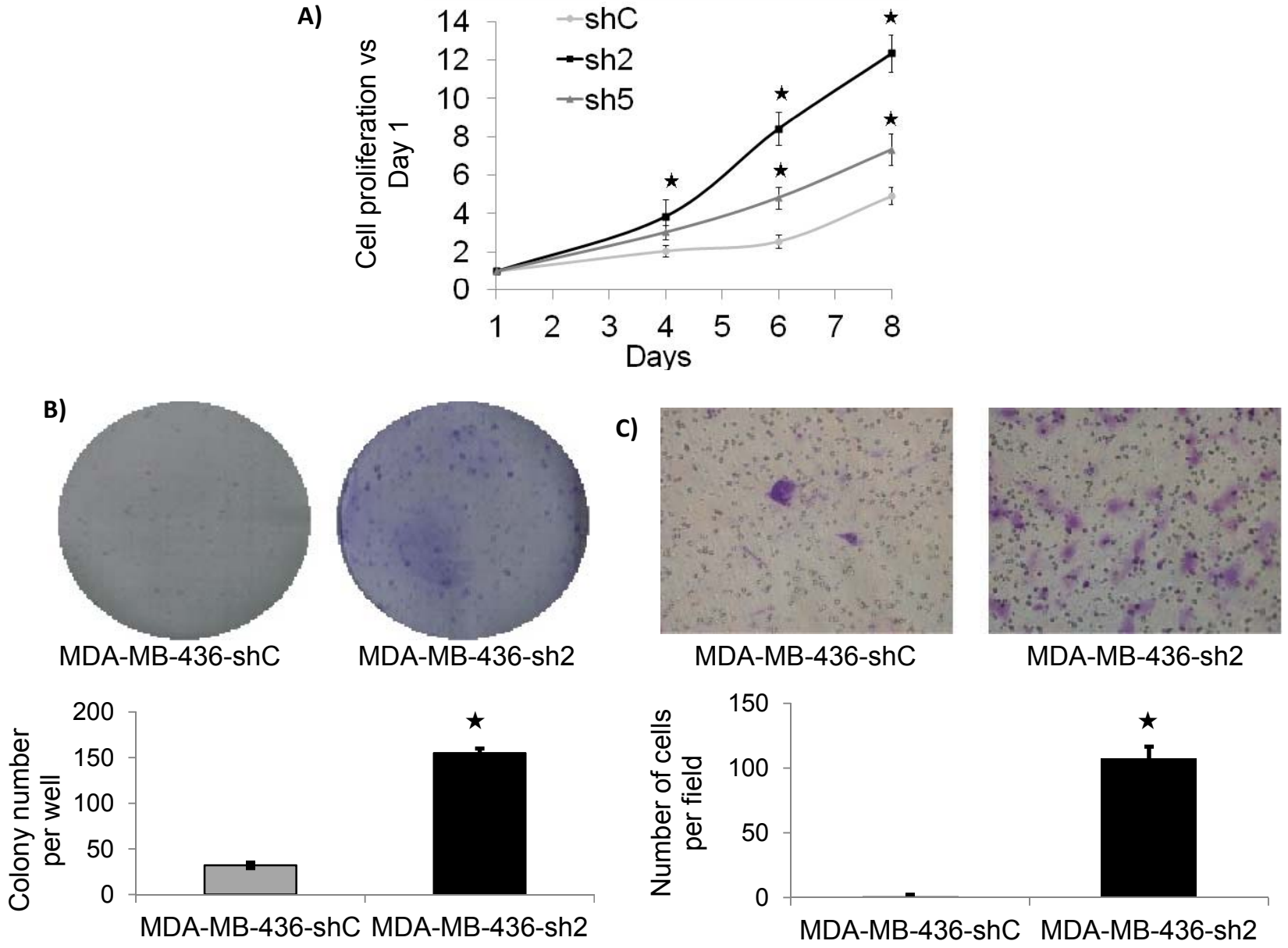
A)
Cell proliferation vs Day 1
shC
sh2
sh5
Days
B)
MDA-MB-436-shC
MDA-MB-436-sh2
C)
MDA-MB-436-shC
MDA-MB-436-sh2
Colony number per well
MDA-MB-436-shC
MDA-MB-436-sh2
Number of cells per field
MDA-MB-436-shC
MDA-MB-436-sh2

Figure 3

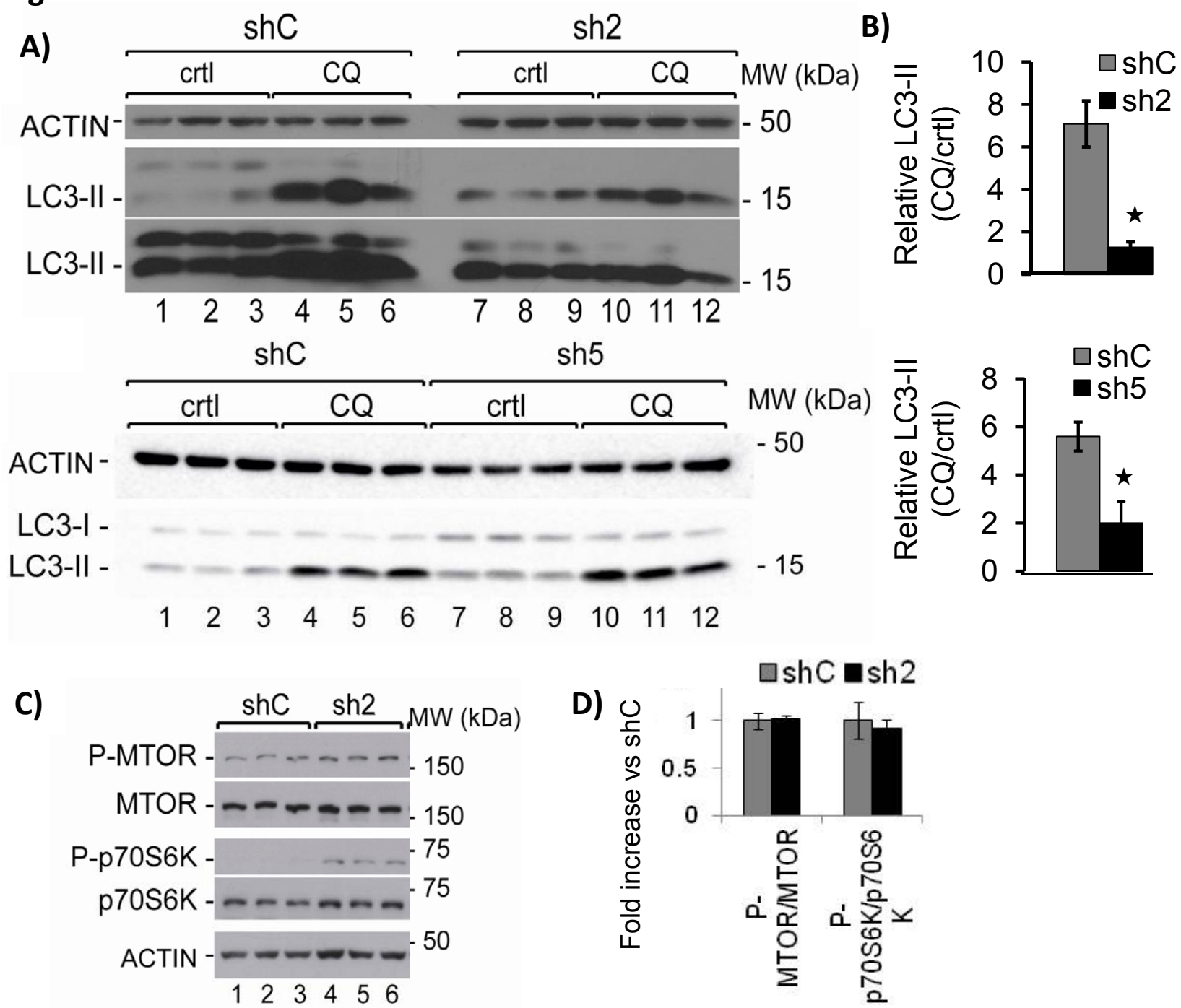
A)
shC
sh2
crtl
CQ
MW (kDa)
ACTIN
LC3-II
- 50
- 15
1 2 3 4 5 6 7 8 9 10 11 12
shC
sh5
LC3-I
LC3-II
B)
Relative LC3-II (CQ/crtl)
shC
sh2
sh5
C)
P-MTOR
MTOR
P-p70S6K
p70S6K
- 150
- 75
D)
Fold increase vs shC
P-MTOR/MTOR
P-p70S6K/p70S6K

Figure 4

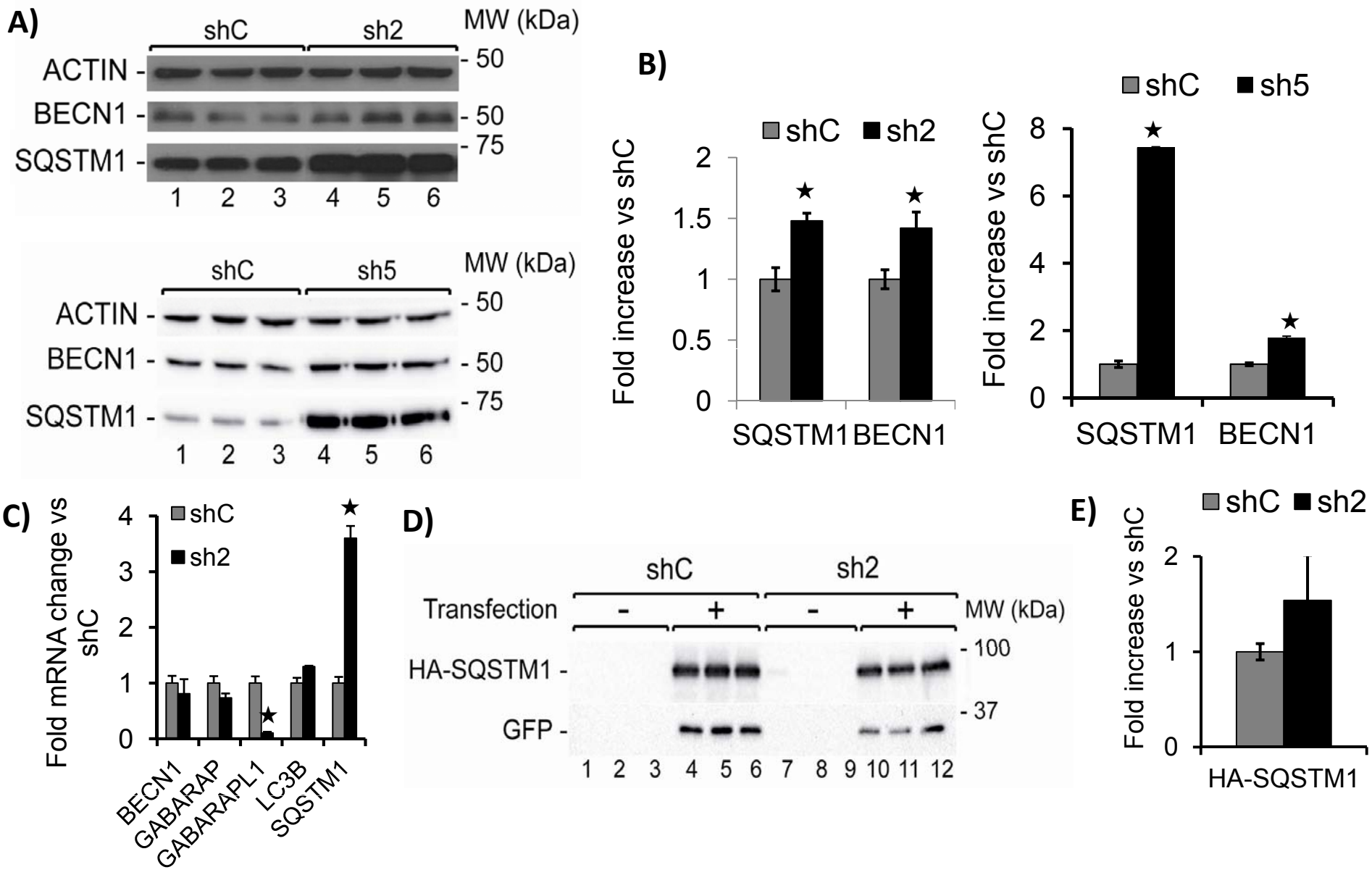
A)
shC
sh2
MW (kDa)
ACTIN -
BECN1 -
SQSTM1 -
- 50
- 50
- 75
1 2 3 4 5 6
shC
sh5
MW (kDa)
ACTIN -
BECN1 -
SQSTM1 -
- 50
- 50
- 75
1 2 3 4 5 6
B)
shC
sh2
Fold increase vs shC
2
1.5
1
0.5
0
SQSTM1 BECN1
shC
sh5
Fold increase vs shC
8
6
4
2
0
SQSTM1 BECN1
C)
Fold mRNA change vs shC
shC
sh2
4
3
2
1
0
BECN1
GABARAP
GABARAPL1
LC3B
SQSTM1
D)
shC
sh2
Transfection
-
+
-
+
MW (kDa)
HA-SQSTM1 -
GFP -
- 100
- 37
1 2 3 4 5 6 7 8 9 10 11 12
E)
shC
sh2
Fold increase vs shC
2
1
0
HA-SQSTM1

Figure 5

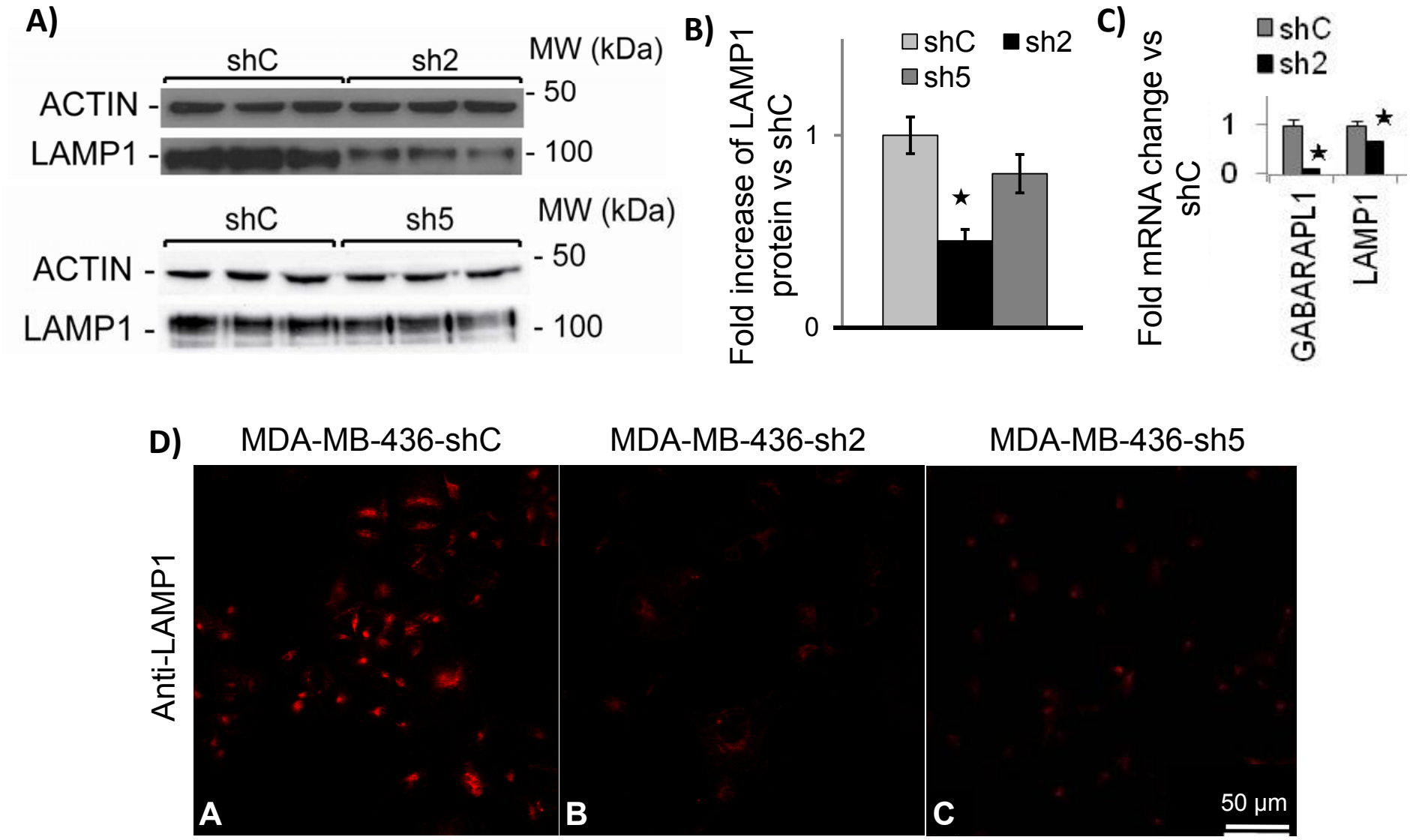
A)
shC
sh2
MW (kDa)
ACTIN -
- 50
LAMP1 -
- 100
shC
sh5
MW (kDa)
ACTIN -
- 50
LAMP1 -
- 100
B)
Fold increase of LAMP1 protein vs shC
1
0
shC
sh2
sh5
C)
Fold mRNA change vs shC
shC
sh2
1
0
GABARAPL1
LAMP1
D)
MDA-MB-436-shC
MDA-MB-436-sh2
MDA-MB-436-sh5
Anti-LAMP1
A
B
C
50 µm

Figure 6

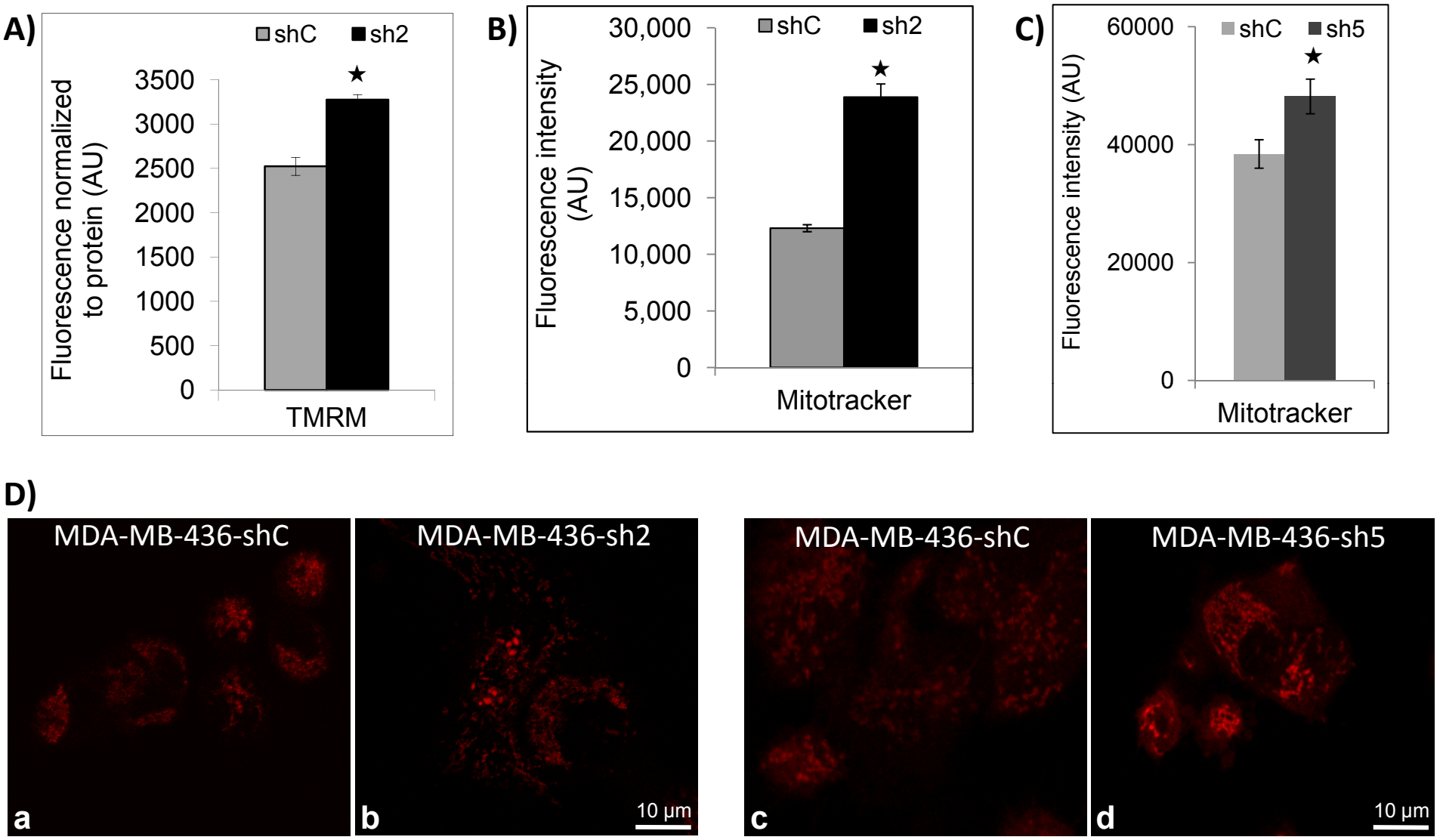
A)
shC
sh2
Fluorescence normalized to protein (AU)
3500
3000
2500
2000
1500
1000
500
0
TMRM
B)
shC
sh2
Fluorescence intensity (AU)
30,000
25,000
20,000
15,000
10,000
5,000
0
Mitotracker
C)
shC
sh5
Fluorescence intensity (AU)
60000
40000
20000
0
Mitotracker
D)
MDA-MB-436-shC
MDA-MB-436-sh2
MDA-MB-436-shC
MDA-MB-436-sh5
a
b
10 µm
c
d
10 µm

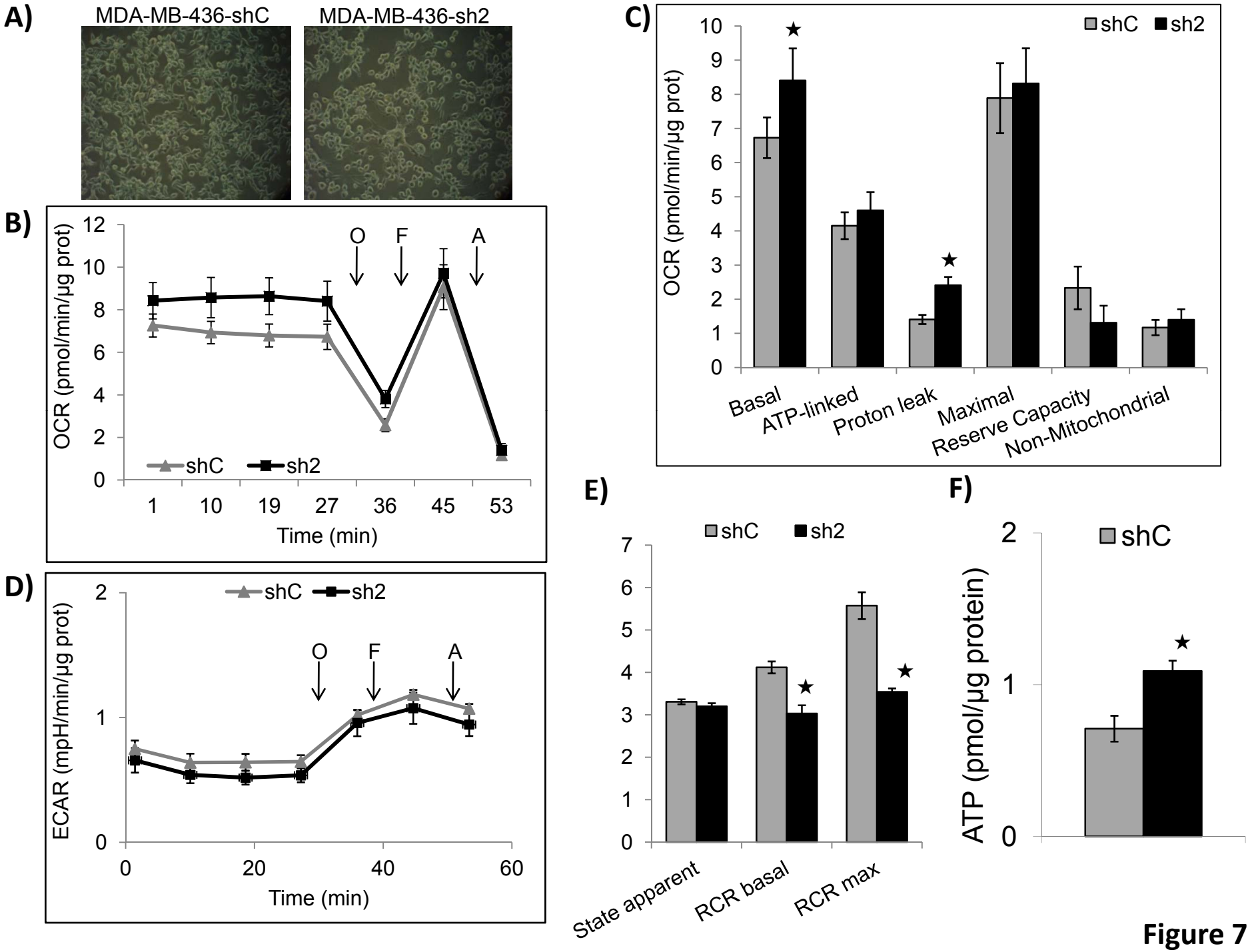
A)
MDA-MB-436-shC
MDA-MB-436-sh2
B)
OCR (pmol/min/µg prot)
O
F
A
shC
sh2
Time (min)
C)
shC
sh2
OCR (pmol/min/µg prot)
Basal
ATP-linked
Proton leak
Maximal
Reserve Capacity
Non-Mitochondrial
D)
shC
sh2
ECAR (mpH/min/µg prot)
O
F
A
Time (min)
E)
shC
sh2
State apparent
RCR basal
RCR max
F)
shC
ATP (pmol/µg protein)

Figure 7

Figure 8

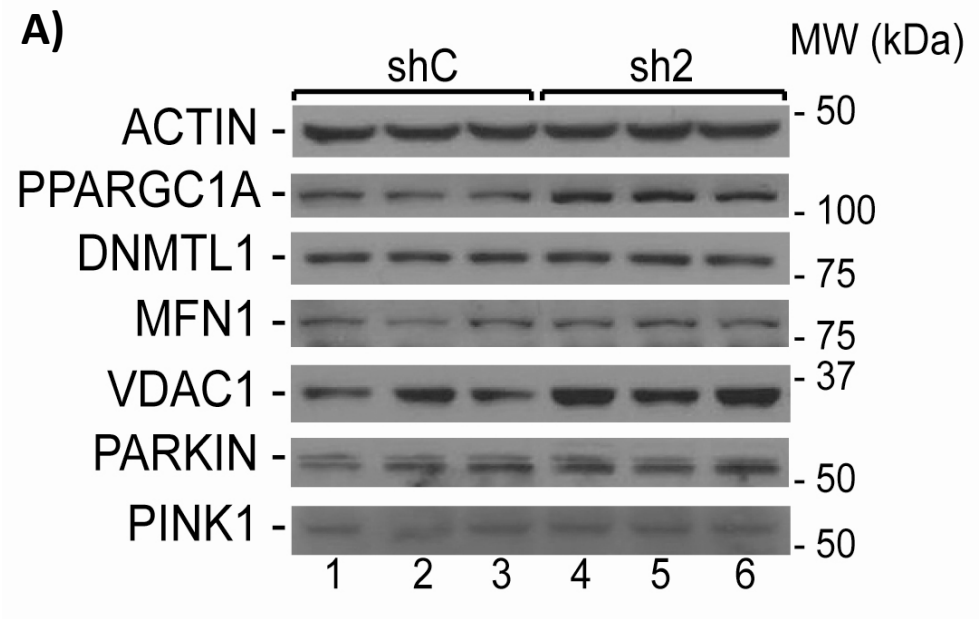
A)
shC
sh2
MW (kDa)
ACTIN -
PPARGC1A -
DNMTL1 -
MFN1 -
VDAC1 -
PARKIN -
PINK1 -
- 50
- 100
- 75
- 75
- 37
- 50
- 50
1 2 3 4 5 6

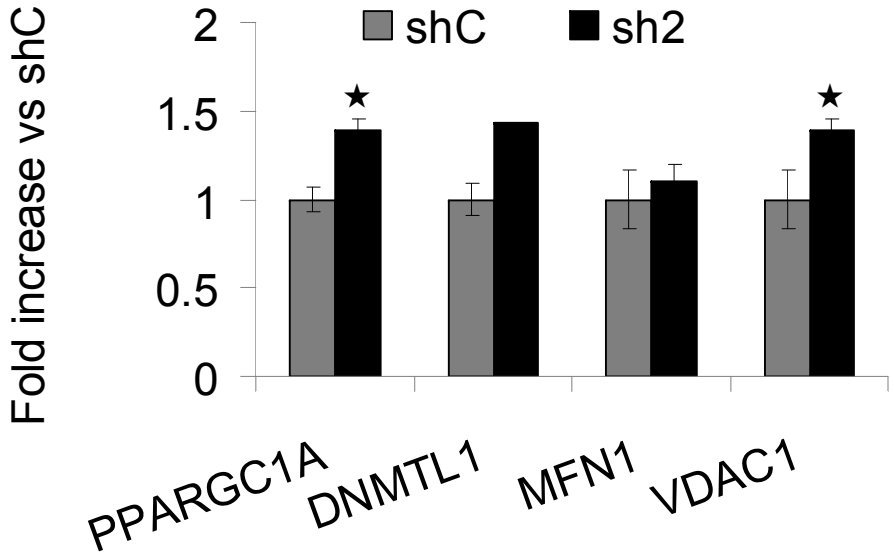
B)
Fold increase vs shC
shC
sh2
2
1.5
1
0.5
0
PPARGC1A
DNMTL1
MFN1
VDAC1

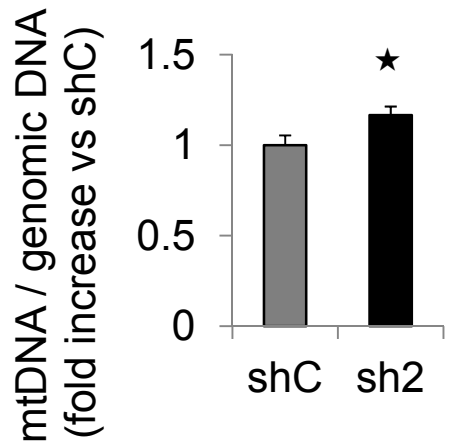
C)
mtDNA / genomic DNA
(fold increase vs shC)
1.5
1
0.5
0
shC
sh2

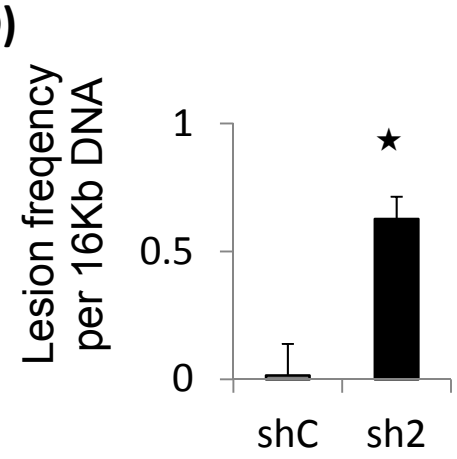
D)
Lesion freqency
per 16Kb DNA
1
0.5
0
shC
sh2

Figure 9

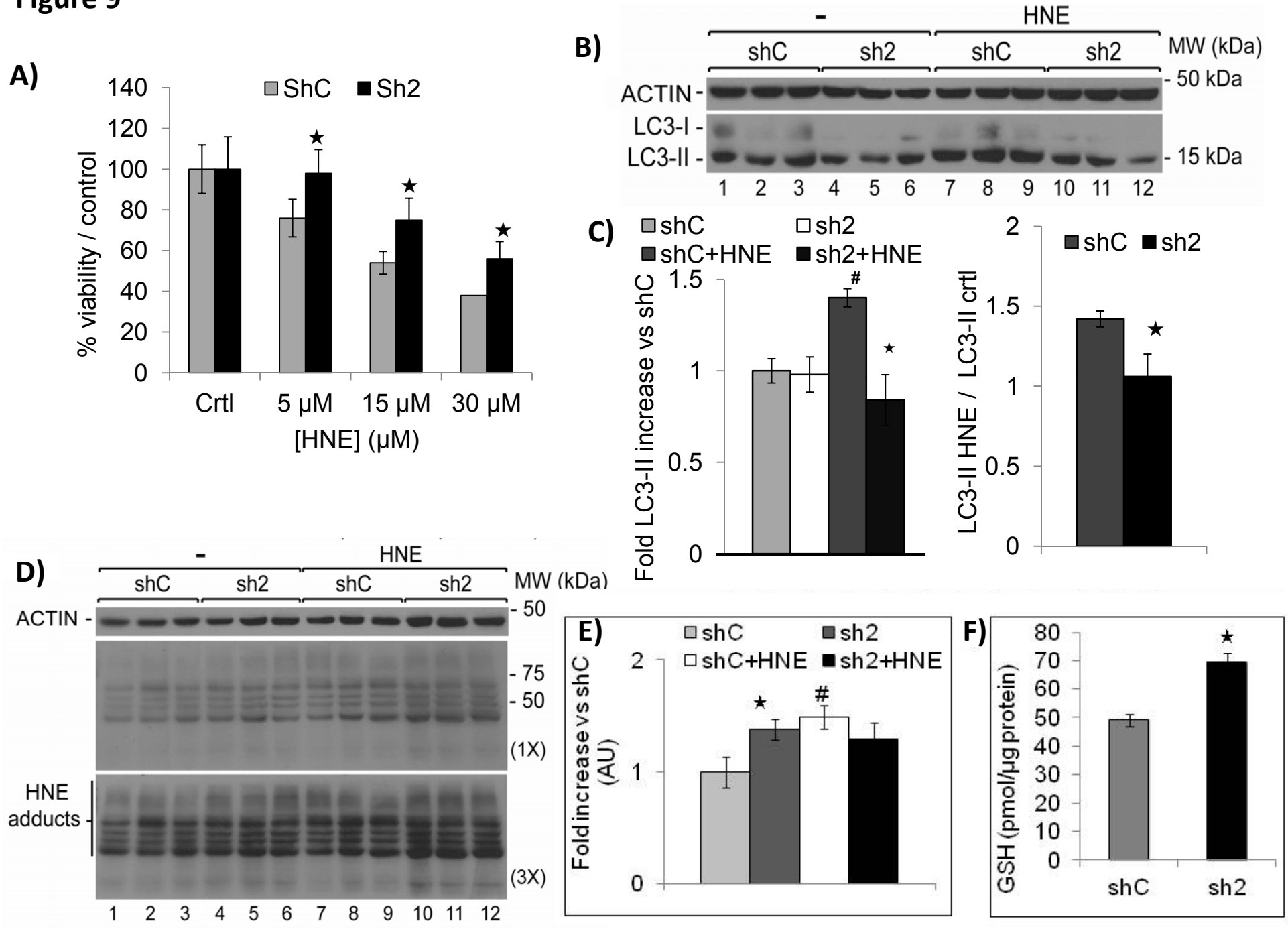
A)
ShC
Sh2
% viability / control
140
120
100
80
60
40
20
0
Crtl
5 µM
15 µM
30 µM
[HNE] (µM)
B)
-
HNE
shC
sh2
shC
sh2
MW (kDa)
ACTIN -
- 50 kDa
LC3-I -
LC3-II -
- 15 kDa
1 2 3 4 5 6 7 8 9 10 11 12
C)
shC
sh2
shC+HNE
sh2+HNE
Fold LC3-II increase vs shC
1.5
1
0.5
0
#
LC3-II HNE / LC3-II crtl
2
1.5
1
0.5
0
D)
-
HNE
shC
sh2
shC
sh2
MW (kDa)
ACTIN -
- 50
- 75
- 50
(1X)
HNE adducts -
(3X)
1 2 3 4 5 6 7 8 9 10 11 12
E)
shC
sh2
shC+HNE
sh2+HNE
Fold increase vs shC (AU)
2
1
0
#
F)
GSH (pmol/µg protein)
80
70
60
50
40
30
20
10
0
shC
sh2

Figure 10

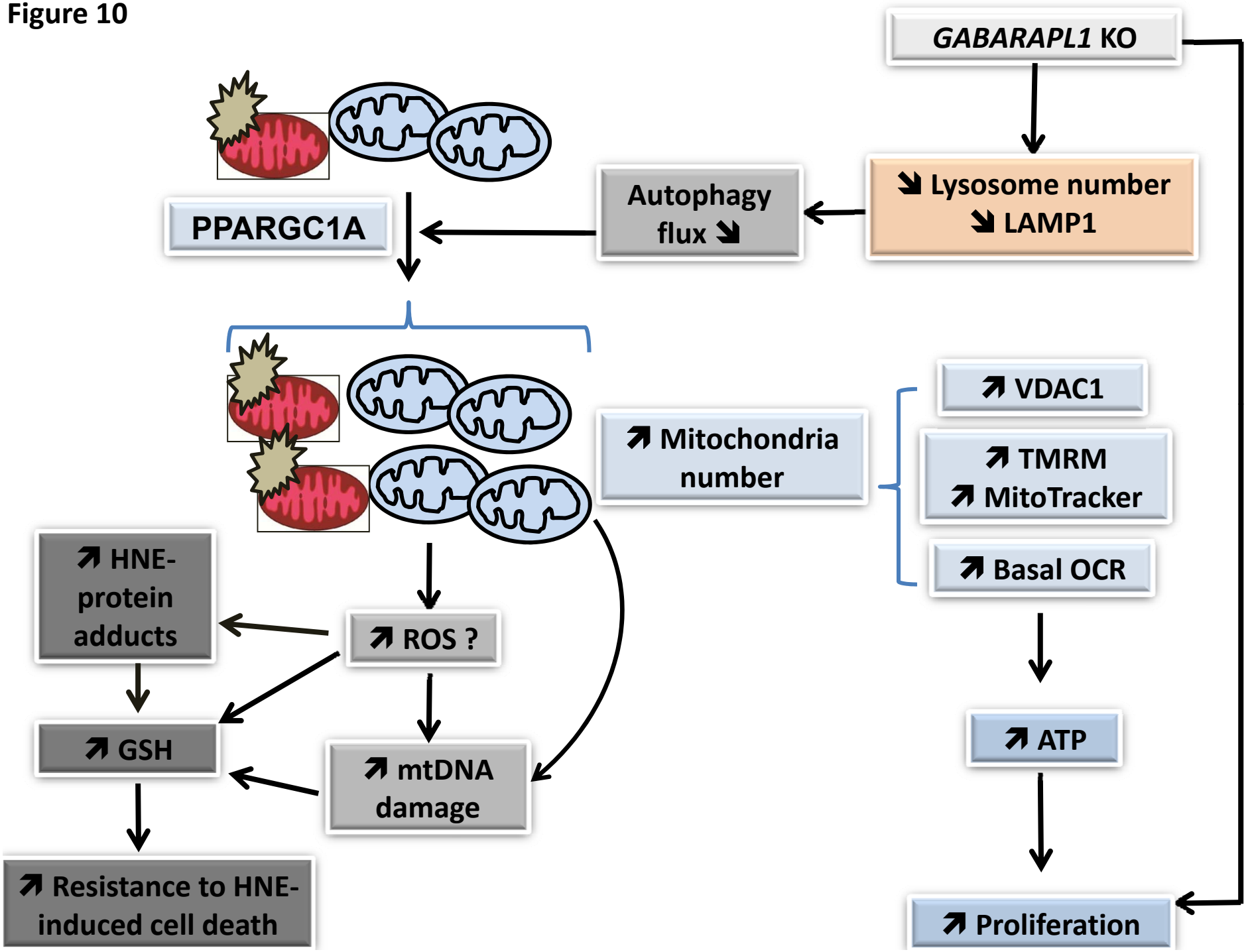
GABARAPL1 KO
↘ Lysosome number
↘ LAMP1
Autophagy flux ↘
PPARGC1A
↗ Mitochondria number
↗ VDAC1
↗ TMRM
↗ MitoTracker
↗ Basal OCR
↗ HNE-protein adducts
↗ ROS ?
↗ GSH
↗ mtDNA damage
↗ ATP
↗ Resistance to HNE-induced cell death
↗ Proliferation